AD-A153 138 ANALYTICAL SHEAR BUCKLING INVESTIGATION OF CURVED COMPOSITE PANELS(U) AIR FORCE INST OF TECH WRIGHT-PATTERSON AFB OH SCHOOL OF ENGINEERING 1/1

UNCLASSIFIED J K MCDANIEL DEC 84 AFIT/GA/AA/84D-5 F/G 12/1 NL

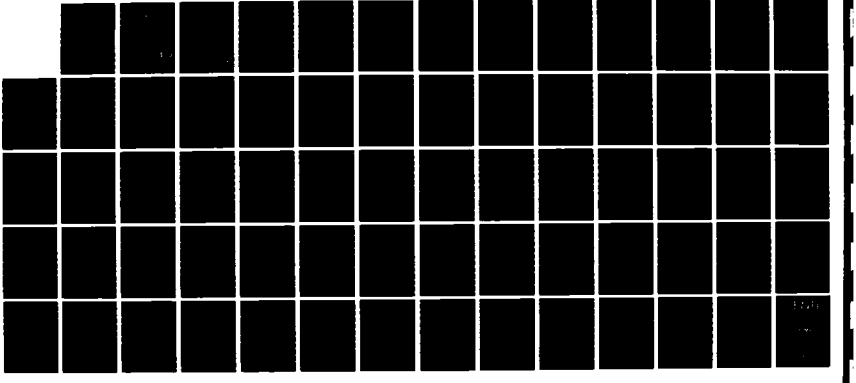

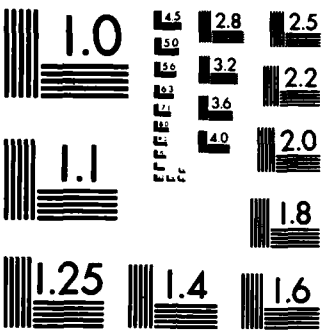

ANALYTICAL SHEAR BUCKLING INVESTIGATION OF CURVED COMPOSITE PANELS

THESIS

Jay K. McDaniel
Captian, USAF

AFIT/GA/AA/84D-5

DEPARTMENT OF THE AIR FORCE
AIR UNIVERSITY
AIR FORCE INSTITUTE OF TECHNOLOGY

Wright-Patterson Air Force Base, Ohio

ANALYTICAL SHEAR BUCKLING INVESTIGATION OF CURVED COMPOSITE PANELS

THESIS

Jay K. McDaniel
Captian, USAF

AFIT/GA/AA/84D-5

AFIT/GA/AA/84D-5

ANALYTICAL SHEAR BUCKLING INVESTIGATION OF CURVED COMPOSITE PANELS

THESIS

Presented to the Faculty of the School of Engineering
of the Air Force Institute of Technology
Air University
in Partial Fulfillment of the
Requirements for the Degree of
Masters of Science

by

Jay K. McDaniel
Captian, USAF
Graduate Astronautical Engineering

December 1984

Acknowledgements

I wish to express my extreme gratitude to Dr. Anthony Palazotto for his patience and expert guidance throughout this thesis.

I would also like to thank the Air Force Flight Dynamics Laboratory, in particular Dr. N. S. Khot and Mrs. Elizabeth Copenhaver, for the support in getting the STAGSC-1 computer code operating on the new ASD Cyber computer system.

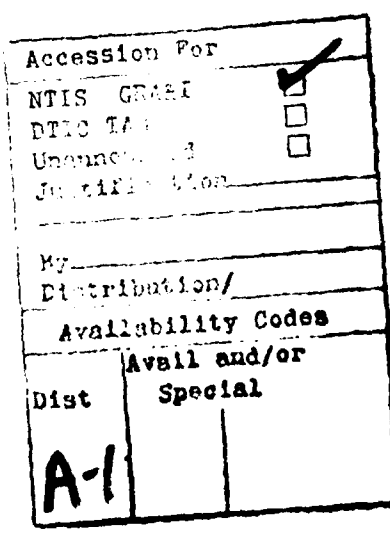

Table of Contents

List of Figures

List of Tables

List of Symbols

A,B,D	Extensional, Coupling, and Bending Stiffness
a	Circumferential Distance
d	Nodal Degree of Freedom
E	Elongation Molulus of Elasticity
G	Shear Modulus of Elasticity
g	Nodal Displacement
H	System Linear Stiffness Matrix
I,J	System Nonlinear Stiffness Matrix
K	Structure Stiffness Matrix
N,M	Inplane Forces and Moments (N also used for total number of lamina)
N1,N2	Matrices with Linear and Quadratic Dependence, Respectively, on Displacement
Q	Reduced Stiffness
Q	Transformed Reduced Stiffness
q	Displacement Vector
R	Structure Applied Loads
Ru,Rv,Rz	Rotations About x, y, and z axes
r	Panel Radius
t	Panel Thickness
u,v,w	Axial, Circumferential, and Radial Displacements
U	Internal Strain Energy
V	Total Potential Energy
W	Work Done by External Forces
x,y,z	Axial, Circumferential, Radial Directions
σ	Stress
ϵ	True Strain

γ	Engineering Strain
ν	Poision's Ratio
θ	Angle Between Material Principle and Natural Axes
κ	Curvatures
ϕ	Rotations
λ	Load Proportionality Parameter
α, β	Nodal Rotations
Subscripts	
i,j,q,r	Nonsummation Indices Equaling 1,2, or 3
x,y	Material Natural Directions
1,2	Material Principal Directions
,	Partial Differentiation
k	Lamina Number
s	Symmetric Laminate
Superscripts	
o	Midplane
T	Transpose

Abstract

This numerical investigation paremetrically determined how material and geometric properties affect the buckling load capability of 8-ply curved composite panels loaded under pure shear. The linear bifurcation capabilities of the STAGSC-1 finite element computer code developed by the Lockheed Palo Alto Research Laboratory was employed. Results from this computer code were compared with other published analytical results of similar configuration to verify boundary conditions.

Representitive material properties for both graphite-epoxy and Kevlar-epoxy were used. The aspect ratios of 0.5, 1.0, and 2.0 were achieved by varying the axial length of the cylindrical panel. Both quasi-isotropic and symmetric orthotropic fiber orientations were analysed.

Results indicate that these curved composite panels, while loaded with a shear load resulting in pure shear reactions in flat plates, do not react in pure shear. Once the interior force resultants are established, the load carrying capability of the curved panels follow classical laminated plate theory.

ANALYTICAL SHEAR BUCKLING INVESTIGATION OF CURVED COMPOSITE PANELS

I. Introduction

Background

As we try to make our vehicles go further, higher, and faster we enevitably run into one requirement; make them lighter and stronger. Many studies on future systems have shown the need for lighter structures. Some examples are the Transatmospheric Vehicle, the Advanced Tactical Fighter, and almost all space systems. This is especially true for any of the space systems since having to get out of the gravity well is expensive.

One possible solution to this problem is the use of composites. Composites provide a light, strong material that can be tailored to the purpose by orienting the fibers to afford strength in desired directions. The composites also promise better fatique life, damage tolarance [10] and can be formed more easily to complex curves. The present problem with composites is the fact that they do not react like isotropic materials. The fact that their stiffness can be oriented to preferred directions make them complex to analyes.

As Whitney states in his latest paper [13], "Numerous papers concerning the instability of laminated, anisotropic plates and shells can be found in the open literature. Buckling of curved panels has, however, received little attention" This is even more the case with shear buckling. The work done in Refs. [2], [3], and [4] is concerned with compressive buckling of curved panels.

Reference [1] deals with shear buckling of an entire cylinder, not a curved panel. In this thesis, a parametric study is performed on a curved composite panel and how the parameters, described next, effect shear buckling loads using a finite element code.

Problem Statement

This study examines the buckling characteristics of a simply supported cylindrical composite panel with a 12 inch radius of curvature loaded in pure shear. The parameters which were varied were aspect ratio, fibre orientations, and material properties. The values for these parameters are presented in chapter 3. The results are analysed and explanations for the trends are formulated in chapter 4.

II. Theory

Bifurcation Buckling vs Collapse Load

The main difference between bifurcation buckling and collapse load (as the terms are used here) is that bifurcation buckling uses the original stiffness matrix computed for the structure through buckling. A collapse load analysis is a nonlinear method that continually updates the stiffness matrix as the structure deforms and takes on new shapes. Both techniques increment the applied load until the point that produces a structural instabillity is reached. This is characterized for a linear prebuckling solution when the structure's equilibrium equations have multiple solutions.

Comparisons of the results of bifurcation and collapse load analysis [8] have indicated when each should be used. The bifurcation analysis normally predicts a lower failure load than does the nonlinear collapse load technique. However, in structures not containing geometric discontinuities, such as holes, the bifurcation analysis provides a fair approximation of the collapse load results. When structures contain geometric discontinuities the nonlinear results indicate that the deformations along the free edges of the hole permit a redistribution of the stresses away from this free edge throughout the structure, thus resulting in a higher load bearing capability.

Since the structures in this thesis are simply supported shells with no cutouts, the linear bifurcation portion of the

STAGSC-1 [6] finite ellement code was employed. The theory for this portion of the code is discussed in the STAGSC-1 Theory section.

Classical Laminated Plate Theory

An understanding of classical laminated plate theory (CLPT) is required whenever dealing with composite structures. This section is intended to provide a brief overview of basic principles. A more complete treatment can be found in any introductory composite text such as [10]. CLPT is presented here for completness.

We begin by discussing the stress-strain relations for a single lamina in plane stress. These relations are given by

$$\begin{Bmatrix} \sigma_1 \\ \sigma_2 \\ \sigma_{12} \end{Bmatrix} = \begin{bmatrix} Q_{11} & Q_{12} & 0 \\ Q_{21} & Q_{22} & 0 \\ 0 & 0 & Q_{66} \end{bmatrix} \begin{Bmatrix} \epsilon_1 \\ \epsilon_2 \\ \gamma_{12} \end{Bmatrix} \tag{1}$$

where:

$$\begin{aligned} Q_{11} &= E_1 / (1-\nu_{12}\nu_{21}) \\ Q_{12} &= \nu_{12} E_2 / (1-\nu_{12}\nu_{21}) \\ Q_{22} &= E_2 / (1-\nu_{12}\nu_{21}) \\ Q_{66} &= G_{12} \end{aligned} \tag{2}$$

Note that the 1 and 2 subscripts denote the principal material direction (see Fig. 1).

For the more general case where the principal material directions do not align with the natural body axes, the reduced stiffness matrix $[Q_{IJ}]$ must be replaced by the transformed reduced stiffness marix $[\bar{Q}_{IJ}]$ where:

$$\bar{Q}_{11}=Q_{11}\cos^4\theta+2(Q_{12}+2Q_{66})\sin^2\theta\cos^2\theta+Q_{22}\sin^4\theta$$

$$\bar{Q}_{12}=(Q_{11}+Q_{22}-4Q_{66})\sin^2\theta\cos^2\theta+Q_{12}(\sin^4\theta+\cos^4\theta)$$

$$\bar{Q}_{22}=Q_{11}\sin^4\theta+2(Q_{12}+2Q_{66})\sin^2\theta\cos^2\theta+Q_{22}\cos^4\theta \qquad (3)$$

$$\bar{Q}_{16}=(Q_{11}-Q_{12}-2Q_{66})\sin\theta\cos^3\theta+(Q_{12}-Q_{22}+2Q_{66})\sin^3\theta\cos\theta$$

$$\bar{Q}_{26}=(Q_{11}-Q_{12}-2Q_{66})\sin^3\theta\cos\theta+(Q_{12}-Q_{22}+2Q_{66})\sin\theta\cos^3\theta$$

$$\bar{Q}_{66}=(Q_{11}+Q\ \ -2Q_{12}-2Q_{66})\sin^2\theta\cos^2\theta+Q_{66}(\sin^4\theta+\cos^4\theta)$$

Note that the $[\bar{Q}_{IJ}]$ matrix is fully populated and the stresses and strains in Eq. (1) are measured along the natural body axes, x and y.

To expand these arguments to a general layered laminate, two assumptions must be made. The first is that the bonds between the lamina are perfect. That is, there is no slipping between laminae. Secondly, the Kirchhoff-Love hypothesis which states

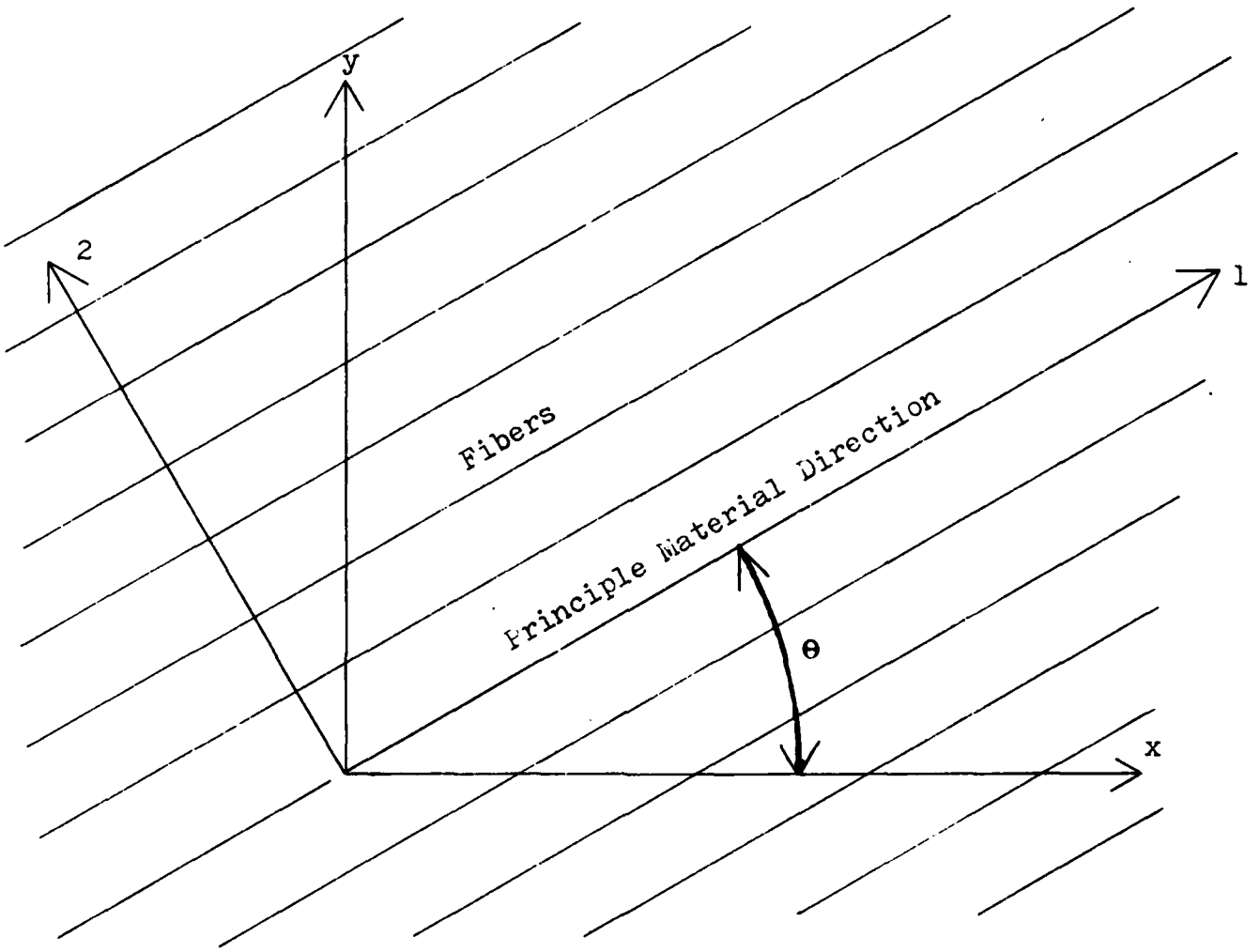

Figure 1. Positive Rotation of Principle Material Axis from Arbitrary x-y axes [10]

that normals to the midsurface remain normal after deformation is enforced throughout the laminate. These assumptions lead to the strain equations

$$\begin{Bmatrix} \epsilon_x \\ \epsilon_y \\ \gamma_{xy} \end{Bmatrix} = \begin{Bmatrix} \epsilon_x^o \\ \epsilon_y^o \\ \gamma_{xy}^o \end{Bmatrix} + z \begin{Bmatrix} \kappa_x \\ \kappa_y \\ \kappa_{xy} \end{Bmatrix} \tag{4}$$

where the o superscripts represent midsurface values and the κ's are midsurface curvatures. The distance from the midsurface perpendicular to the x-y plane is given by z as shown in Fig. 2.

The above strains and curvatures are given by Sanders' kinematic relations [9] for a cylindrical panel with moderately large displacements and rotations of tangents to the midsurface by

$$\begin{aligned} \epsilon_x^o &= u_{,x} + 0.5\phi_x^2 + 0.5\phi^2 \\ \epsilon_y^o &= v_{,x} + (w/r) + 0.5\phi_y^2 - 0.5\phi \\ \gamma_{xy}^o &= v_{,x} + u_{,y} + \phi_x\phi_y \\ \kappa_x &= \phi_{x,x} \\ \kappa_y &= \phi_{y,y} \\ 2\kappa_{xy} &= \phi_{y,x} + \phi_{x,y} + \phi/r \end{aligned} \tag{5}$$

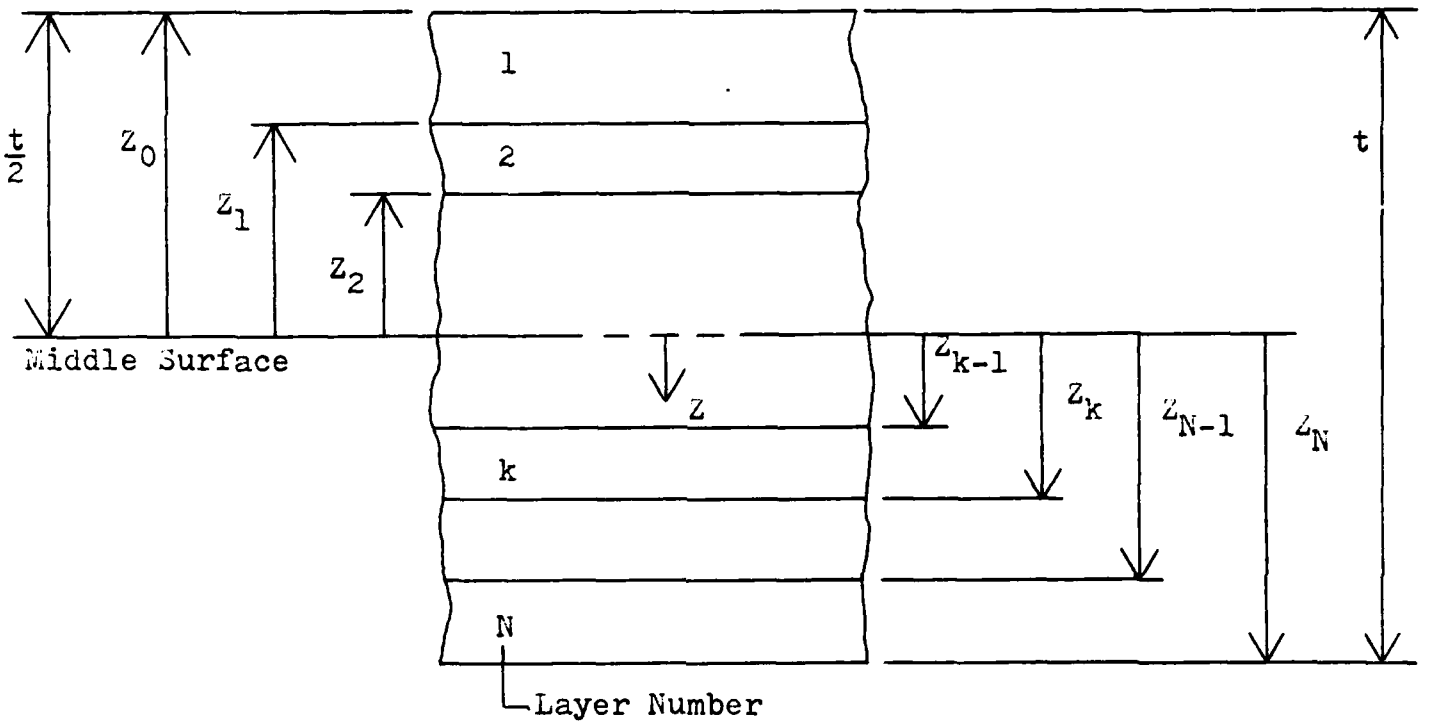

Figure 2. Geometry of an N-Layered Laminate [10]

where u, v, and w are the axial, circumferential, and radial displacements, respectively, of the panel's midsurface. The r is the panel's radius of curvature. The ϕ's are rotations expressed as:

$$\phi_x = -w_{,x}$$

$$\phi_y = -w_{,y} + (v/r) \tag{6}$$

$$\phi = 0.5(v_{,x} - u_{,y})$$

Note that the commas in the subscripts denote partial differentiation with respect to the parameter that follows the comma.

The stresses in the k^{th} lamina can be expressed in terms of the midsurface strains and curvatures by substituting Eq. (4) into Eq. (1) (with the transformed reduced stiffness matrix) resulting in:

$$\begin{Bmatrix} \sigma_x \\ \sigma_y \\ \sigma_{xy} \end{Bmatrix}_k = \begin{bmatrix} Q_{11} & Q_{12} & Q_{16} \\ Q_{21} & Q_{22} & Q_{26} \\ Q_{61} & Q_{62} & Q_{66} \end{bmatrix}_k \left(\begin{Bmatrix} \epsilon_x^o \\ \epsilon_y^o \\ \gamma_{xy}^o \end{Bmatrix} + z \begin{Bmatrix} \kappa_x \\ \kappa_y \\ \kappa_{xy} \end{Bmatrix} \right) \tag{7}$$

The resultant forces and moments per unit width acting on a laminate as shown in Fig. 3 are now obtained by integrating the stresses in each lamina through the laminate thickness, as:

$$N_x = \int_{-t/2}^{t/2} \sigma_x dZ$$

$$M_x = \int_{-t/2}^{t/2} \sigma_x Z dZ \tag{8}$$

All the forces and moments shown in Fig. 3 can be written as

$$\begin{Bmatrix} N_x \\ N_y \\ N_{xy} \end{Bmatrix} = \int_{-t/2}^{t/2} \begin{Bmatrix} \sigma_x \\ \sigma_y \\ \sigma_{xy} \end{Bmatrix} dZ = \sum_{k=1}^{N} \int_{Z_{k-1}}^{Z_k} \begin{Bmatrix} \sigma_x \\ \sigma_y \\ \sigma_{xy} \end{Bmatrix}_k dZ$$

$$\begin{Bmatrix} M_x \\ M_y \\ M_{xy} \end{Bmatrix} = \int_{-t/2}^{t/2} \begin{Bmatrix} \sigma_x \\ \sigma_y \\ \sigma_{xy} \end{Bmatrix} Z dZ = \sum_{k=1}^{N} \int_{Z_{k-1}}^{Z_k} \begin{Bmatrix} \sigma_x \\ \sigma_y \\ \sigma_{xy} \end{Bmatrix}_k Z dZ \tag{9}$$

where N is the total number of laminae and Z_k and Z_{k-1} are defined in Fig. 2.

One can now substitute Eq. (7) into Eq. (9) to arrive at an expression for the force and moment resultants in terms of the transformed reduced stiffness matrix and the midplane strains and curvatures. Since the stiffness matrix is constant over the lamina, it can come out from under the integration sign. Also note that the midplane strains and curvatures are independent of Z; therefore, they can be removed from under the integration and summation signs. Thus, the force and moment resultants can be written as

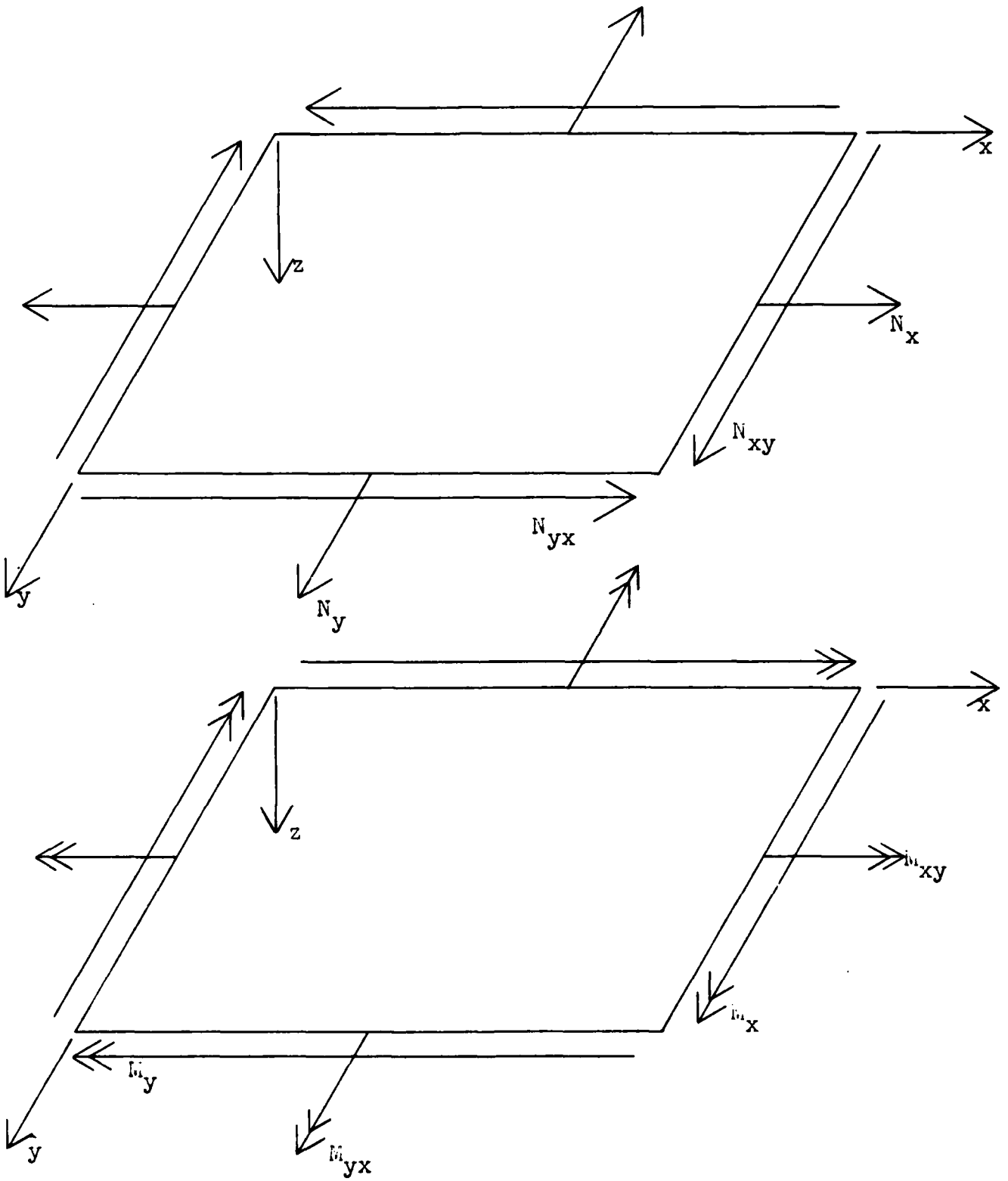

Figure 3. Inplane Forces and Moments for a Laminate

$$\begin{Bmatrix} N_x \\ N_y \\ N_{xy} \end{Bmatrix} = \begin{bmatrix} A_{11} & A_{12} & A_{16} \\ A_{21} & A_{22} & A_{26} \\ A_{61} & A_{62} & A_{66} \end{bmatrix} \begin{Bmatrix} \epsilon_x^o \\ \epsilon_y^o \\ \gamma_{xy}^o \end{Bmatrix} + \begin{bmatrix} B_{11} & B_{12} & B_{16} \\ B_{21} & B_{22} & B_{26} \\ B_{61} & B_{62} & B_{66} \end{bmatrix} \begin{Bmatrix} \kappa_x \\ \kappa_y \\ \kappa_{xy} \end{Bmatrix}$$

$$\begin{Bmatrix} M_x \\ M_y \\ M_{xy} \end{Bmatrix} = \begin{bmatrix} B_{11} & B_{12} & B_{16} \\ B_{21} & B_{22} & B_{26} \\ B_{61} & B_{62} & B_{66} \end{bmatrix} \begin{Bmatrix} \epsilon_x^o \\ \epsilon_y^o \\ \gamma_{xy}^o \end{Bmatrix} + \begin{bmatrix} D_{11} & D_{12} & D_{16} \\ D_{21} & D_{22} & D_{26} \\ D_{61} & D_{62} & D_{66} \end{bmatrix} \begin{Bmatrix} \kappa_x \\ \kappa_y \\ \kappa_{xy} \end{Bmatrix} \qquad (10)$$

where:

$$A_{ij} = \sum_{k=1}^{N} (Q_{ij})_k \ (z_k - z_{k-1})$$

$$B_{ij} = 0.5 \sum_{k=1}^{N} (Q_{ij})_k \ (z_k^2 - z_{k-1}^2) \qquad (11)$$

$$D_{ij} = 0.3 \sum_{k=1}^{N} (Q_{ij})_k \ (z_k^3 - z_{k-1}^3)$$

The A_{ij} are called extensional stiffnesses, the B_{ij} are called coupling stiffnesses, and the D_{ij} are called bending stiffness.

It is noted here that all the panels considered in this thesis have symmetric layups about the midplane. This results in no coupling between extension and bending since the B matrix is a null matrix from the above equations. The equations for A_{ij} and D_{ij} are used in subsequent sections to explain the numerical results.

STAGSC-1 Theory

The Structural Analysis of General Shells (STAGSC-1) computer code [5, 6, 7] is a finite element approach based on the principle of minimum potential energy. The principle of minimum potential energy states that [11]:

> "Among all admissible configurations of a conservative system, those that satisfy the equations of equilibrium make the potential energy stationary with respect to small variations of displacement. If the stationary condition is a minimum, the equation state is stable."

Loss of stability (bifurcation) occurs when the second variation of a systems' total potential energy ceases to be positive definite. The following discussion outlines how STAGSC-1 establishes the bifurcation load through an eigenvalue technique. This discussion can also be found in Ref. [2].

A shell's total potential energy is given by

$$V=U-W \tag{12}$$

where V is the total potential energy, U is the internal strain energy, and W is the work done by external forces. This can also be written as [11]

$$V=0.5 \left|d\right|^{T} [K] \left|d\right| - \left|d\right|^{T} \left|R\right| \tag{13}$$

where $\left|d\right|$ is nodal degree of freedom of the structure vector, [K] is the structure stiffness matrix, $\left|R\right|$ is the structural applied load vector.

For a composite panel, the element strain energy is given by [9]

$$U=0.5\sum_{k=1}^{N}\iint_{S}\left|\epsilon\right|_{o}^{T}\begin{bmatrix}[A] & [B]\\ [B] & [D]\end{bmatrix}\left|\epsilon\right|_{o}\,dS \tag{14}$$

Where [A], [B], and [D] are the 3x3 stiffness matrices given by Eq. (11), the $\left|\epsilon\right|_{o}$ is the midplane strain and curvature vector given by Eqs. (5) and (6), N is the number of lamina in the laminate, and S is the surface area.

Examination of Eqs. (5) and (6) reveals that the strain vector is a function of the midplane displacements, their first partial derivatives with respect to x and y, and their second partial derivatives of w with respect to x and y. Bauld [9] carried out the integration of Eq. (14) and found that this expression for the strain energy consisted of three distinct parts. The first was quadratic in displacements, the second was cubic in displacements, and the third was quartic in displacements. This result was written in terms of the appropriate element shape functions and nodal degrees of freedom to get the form of Eq. (13). The result for the total potential energy is then [9]

$$V=(0.5H_{qr}+0.16N1_{qr}+0.083N2_{qr})q_q q_r-R_r q_r \tag{15}$$

where the structure nodal degrees of freedom are replaced by the displacement vector, q. H_{qr} is the system's linear stiffness matrix with no dependence on the displacement vector, q. $N1_{qr}$ and

$N2_{qr}$ are matrices with linear and quadratic dependence, respectively, on displacement.

From the previous statement of the principle of total potential energy, setting the first variation of Eq. (15) equal to zero gives:

$$(H_{qr}+0.5N1_{qr}+0.3N2_{qr})q_r-R_q=0 \tag{16}$$

The following expression is found by satisfying the condition for bifurcation and taking the second variation of the total potential energy, and finding the point where it is no longer positive definate:

$$DET\ (H_{qr}+N1_{qr}+N2_{qr})=0 \tag{17}$$

Equation (17) is used by STAGSC-1 to solve the eigenvalue problem of the form

$$[H]+\lambda[I]+\lambda^2[J]=0 \tag{18}$$

where [I] and [J] represent nonlinear stiffness matrices in unknown displacements and products of displacements, respectively. For a linear analysis, λ , is the proportionality constant of a convenient load level used in the equilibrium Eq. (16) to solve for the unknown displacements. The J matrix, which arises from the prebuckling rotations,is often omitted as it will be here. The quantities H and I or equivalently, H and $N1_{qr}$ are

calculated once based on the equilibrium displacements. Finally, the load proportionality parameter, λ, is incremented until a sign change on the left side of Eq. (17) occurs, signifying bifurcation.

III. Modelling

Boundary Conditions and Loading

Figure 4 is a sketch depicting the panel analysed. The boundary conditions were such that a simply supported panel in pure shear was modeled. To accomplish this, displacements in the v direction (circumferential) were allowed to move on all sides except the bottom. This was to prevent free body motion. All other displacements remained fixed. The only rotations allowed were those along the edges in the direction of the edge and all rotations normal to the panel (Rw).

The loads applied as shown in Fig. 4 were line loads. That is, they have units of force/unit length. As such, the applied forces N_{xy} and N_{yx} were equal around the panel. This assured equilibrium and load continuity around the panel.

With this combination of loads and boundary conditions, the only load that was actually applied to the panel was the one along the top of the panel. This is due to the fact that fixed boundry conditions override applied loads in the STAGSC-1 computer code.

Grid Selection

Both references [1] and [2] indicate that for accuracy at least five nodes should be present in each half sine wave of the deformed panel. Initial computer runs provided data indicating that 0.5 inch grids would be required to provide these five nodes. This grid size was used for aspect ratios of 0.5 and 1.0

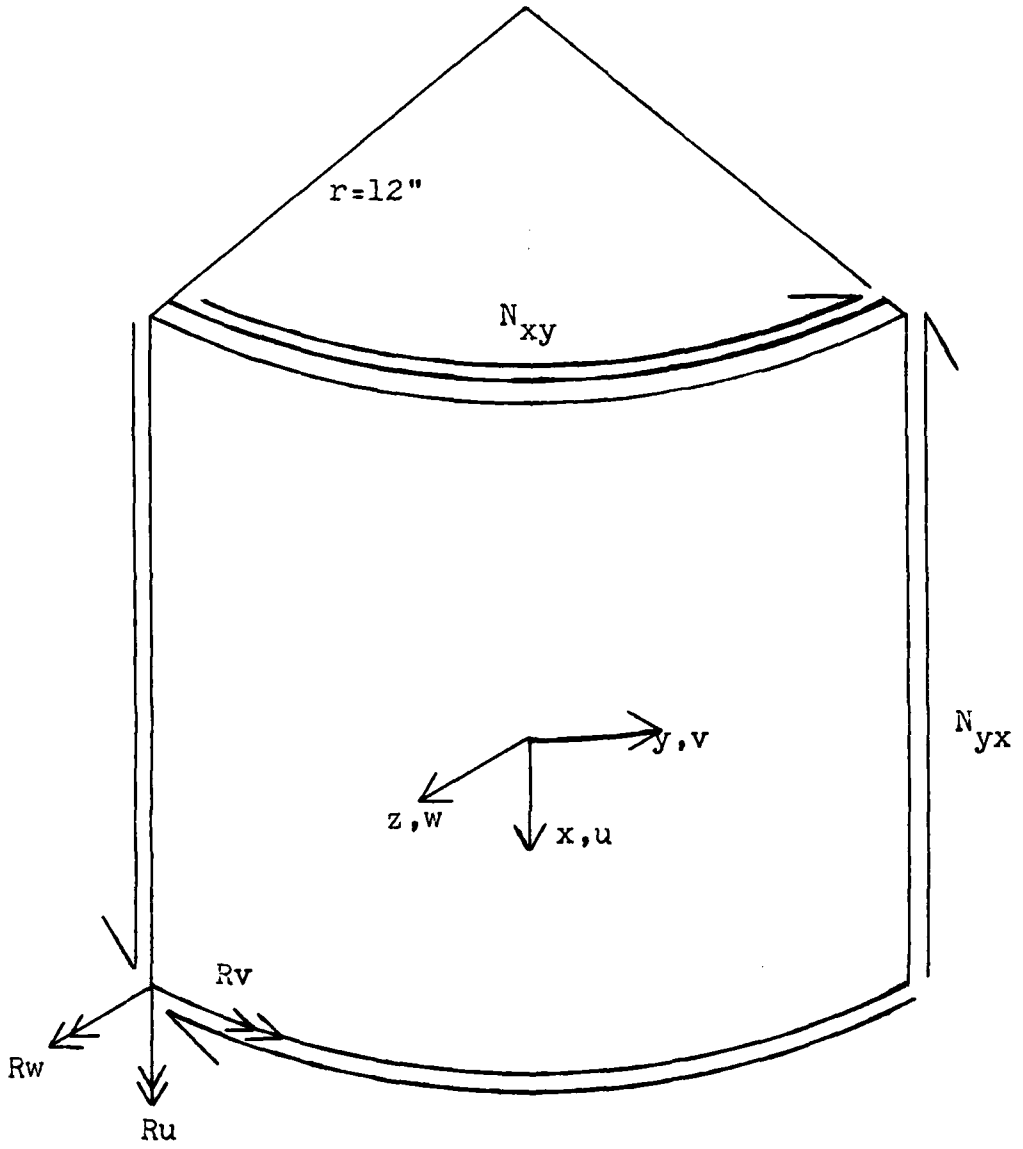

Figure 4. Boundary Conditions and Applied Loads

but a grid size of 1.0 inch was used for the aspect ratio of two. This was to conserve computer time. A comparison to a grid size of 0.5 inch proved no appreciable loss of accuracy.

Aspect Ratios

Three aspect ratios were investigated. These were 0.5, 1.0, and 2.0. Aspect ratio is defined as the axial length (x) divided by the circumferential length (y). The circumferential length remained a constant 12 inches while the axial length was 6, 12, and 24 inches. This was an attempt to investigate only aspect ratio effects on buckling and not curvature effects.

Lamina Orientations

Three lamina orientations were investigated. These were $[0,+45,-45,90]_s$, $[0,90]_{2s}$, and $[+45,-45]_{2s}$. These provided three symmetric orientations with widely varying shear coupling stiffness terms A_{16}, A_{26}, D_{16}, and D_{26} terms. It will be shown in a later chapter what the values of these coefficients are and how they affect the buckling load.

Element Selection

STAGSC-1 has two elements well suited for modeling a curved panel, the QUAF 410 and QUAF 411 elements [6]. Though Ref. [2] indicates the QUAF 410 element would have sufficed for this linear study, the QUAF 411 element was selected to ensure accuracy. This element and the degrees of freedom are shown in Fig. 5.

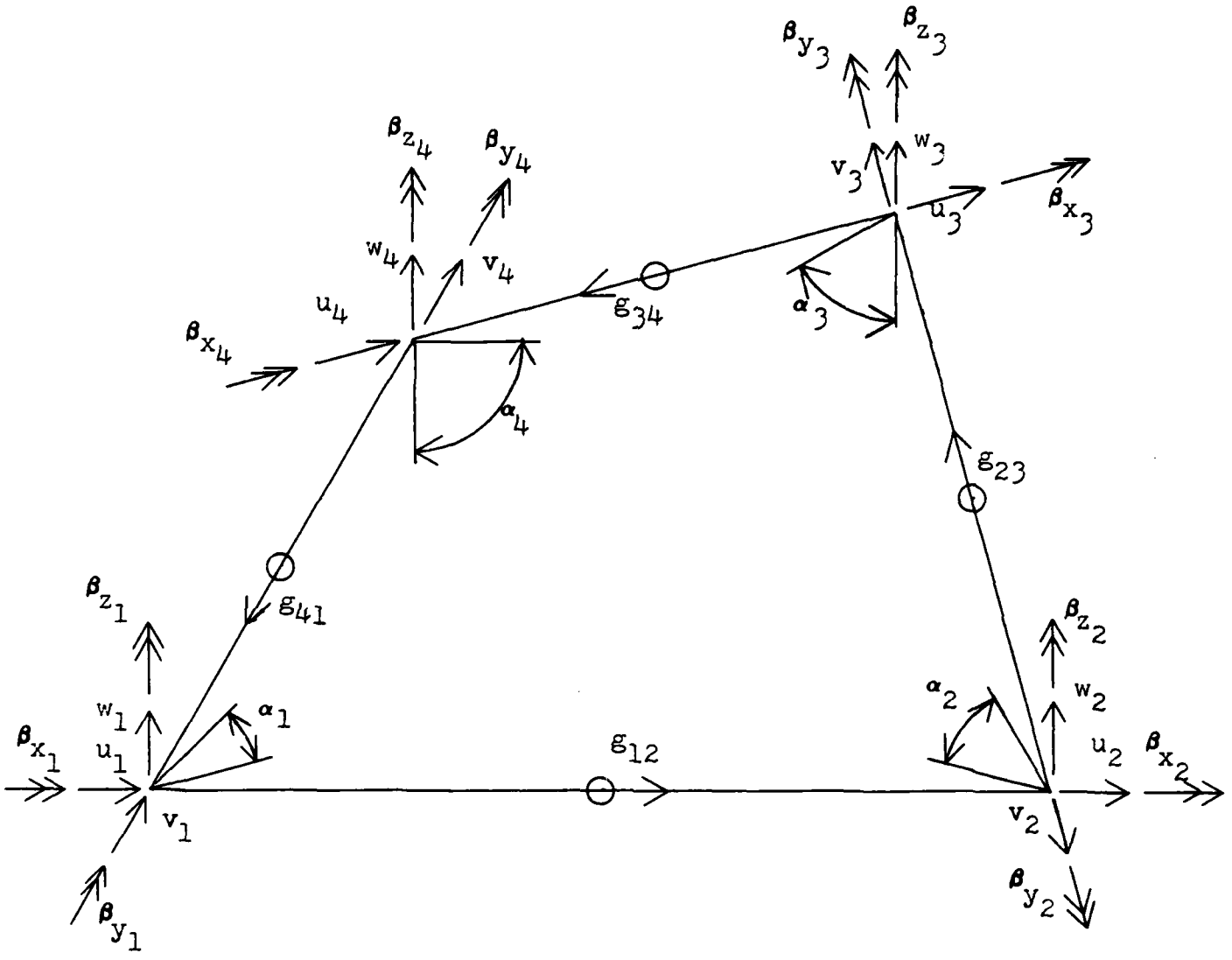

Figure 5. QUAF 411 Ellement

The additional midside tangential displacement degree of freedom, g_{ij}, and the rotational degree of freedom of the edges meeting at a node, α, make the 411 element better suited for nonlinear analysis of cylindrical panels by permitting shear strain matching at the corners [7]. This is an additional characteristic the 410 element does not posses since it is a flat element. Thus, the 411 element is better suited to a cylindrical shell. This is done by insuring the transverse displacement shape functions are of the same order as the in-plane shape functions. Therefore the in-plane shape functions are cubic by introducing the first normal rotation, β_z, at the corners.

Material Selection

The two materials used in this analysis are graphite/epoxy and kevlar/epoxy. The material properties for the graphite/epoxy were the same used in Refs. [2], [3], and [4]. These are:

E_1 =20500 ksi

E_2 = 1300 ksi

G_{12}= 750 ksi

ν_{12}= 0.33

The material properties for kevlar/epoxy were found experimentally in Ref. [14]. These are:

E_1 =10700 ksi

E_2 = 600 ksi

G_{12}= 200 ksi

ν_{12}= 0.25

Flat Plate Check

To check to see if the boundary conditions and loading geometry represent a simply suported panel in pure shear, a comparision was carried out of the results arrived at with STAGSC-1 with the analytic results of a flat square panel [12]. The analytic solution of the flat plate buckling is a Galerkin series solution.

To match the stiffness criterion given for the analytic solution, the material properties had to be changed to:

E_1 =20500 ksi

E_2 = 2050 ksi

G_{12}= 1370 ksi

ν_{12}= 0.33

Also, all eight plies of the panel were changed to a zero orientation since the analysis was on an orthotropic plate. Finally, the radius of curvature of the panel was increased to 24 inches to better simulate a flat plate. All other parameters were kept the same as in the baseline panel with aspect ratio 1.0.

The Galerkin method arrived at a buckling load for the flat plate of N_{xy}=23.7 #/in. The STAGSC-1 analysis obtained a buckling value of N_{xy}=60 #/in. The diferrence in the predicted loads can be attributed to two things. First, even thouqh the radius of curvature was increased to 24 inches, the curved panel should be able to carry more load then the flat plate. Secondly, the flat plate analysis does not take into consideration the membrane stresses that the STAGSC-1 analysis does. Under the applied shear load, these membrane stresses will be tension thus producing a

higher load carrying capability.

It is shown in chapter 4 that a curved composite panel does not react as a flat plate does under pure shear. Looking back at this analysis shows that 24 inches is sufficient curvature to prevent a pure shear reaction. Hence, these results are misleading. The next check better approximates a flat plate with a larger radius of curvature.

Curved Panel Check

Similar to the flat plate check, a comparison of the STAGSC-1 analysis was made to a curved panel analytical solution to check boundary conditions and loading geometry [13]. This was also a Galerkin method solution.

The material properties had to again be modified to meet the analytic analysis. This time the material properties are:

E_1 =20500 ksi

E_2 = 1500 ksi

G_{12}= 730 ksi

ν_{12}= 0.25

The radius of curvature of the panel also had to be increased to 40 inches to avoid extrapolating the documented results. All other parameters were the same as the $[+45,-45]_{2s}$ baseline panel with an aspect ratio of one.

The analytical Galerkin method gave a bifurcation applied stress of σ_{xy} =3000 psi. The STAGSC-1 analysis again gave a higher value of σ_{xy} =3650 psi. This difference can again be explained by the Galerkin method not taking membrane stresses into account.

The bifurcation eigenvectors and stress distribution for this panel are shown in Fig. 6. The eigenvectors are oriented at 45° as would be expected for a flat plate loaded under pure shear. The stress distribution also reflects a panel in pure shear. This indicates the boundary and loading conditions are adequate to model a flat plate in pure shear. That is, a curved panel with a radius of curvature of 40 inches can be considered a flat plate.

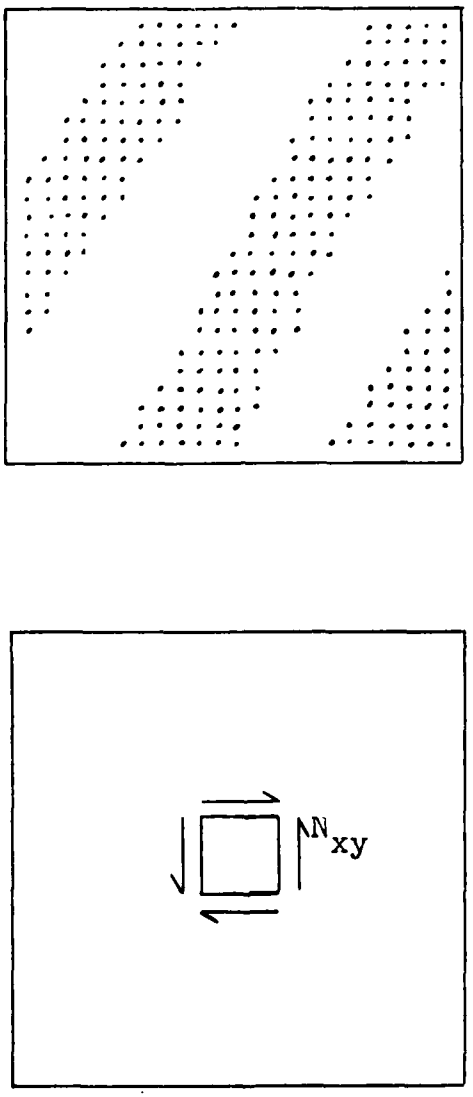

Figure 6. Eigenvectors for and Stress Distribution Throughout $[\pm 45]_{2s}$ Panel with 40 Inch Radius of Curvature. Dots Represent Negative Radial Displacements

IV. Results

Numerical Analysis Results

The ASD Cyber computer system was used to implement the STAGSC-1 computer code. A sample of the input decks used is shown in Appendix A. Table 1 shows the bifurcation load computed for all the panel configurations studied.

The eigenvalue routine that the STAGSC-1 code uses computes all eigenvalues, both positve and negative. The values in Table 1 are the smallest positive values. These correspond to the first bifurcation load. The negative values have no physical significance. They are merely mathematical anomales. It was noted in the computer output that a negative eigenvalue normally occurred with approximately the same magnitude as each positive eigenvalue.

Examination of Table 1 shows a few general trends. First, the results for graphite-epoxy are consistantly higher than those for the Kevlar-epoxy. This is directly attributable to the higher material stiffness properties of the graphite-epoxy over the Kevlar-epoxy. Secondly, the bifurcation load decreases with increasing aspect ratio. This is due to the increase in panel area with the increasing area ratio. It is physically obvious that an infinitly larger panel will not be able to carry a large line load, N_{xy} , since the side length goes to infinity. Similarlly, an infinitly small panel will be able to carry a very large line load, N_{xy}, since the side length goes to zero. This is in line with the results found in Ref. [12]. Lastly, the bifurcation load for the $[+45,-45]_{2s}$ is the highest with the

Aspect Ratios	Fiber Orientations $[0,+45,-45,90]_s$	$[0,90]_{2s}$	$[+45,-45]_{2s}$
0.5	Gr-Ep 271 #/in / Ke-Ep 135 #/in	Gr-Ep 190 #/in / Ke-Ep 87.1 #/in	Gr-Ep 379 #/in / Ke-Ep 184 #/in
1.0	Gr-Ep 188 #/in / Ke-Ep 93.1 #/in	Gr-Ep 133 #/in / Ke-Ep 55.6 #/in	Gr-Ep 253 #/in / Ke-Ep 117 #/in
2.0	Gr-Ep 148 #/in / Ke-Ep 72.9 #/in	Gr-Ep 125 #/in / Ke-Ep 51.3 #/in	Gr-Ep 192 #/in / Ke-Ep 87.5 #/in

Table I. Bifurcation Buckling Load for Composite Panels

$[0,+45,-45,90]_s$ next and the $[0,90]_{2s}$ panel being the weakest. This corresponds to the order of the largest to smallest value for the D_{16} and D_{26} stiffness terms (see Appendix B). This is expected due to the loading applied to the panels.

The eigenvectors are represented graphically in Figs. 7 thru 12. These figures are 2-dimensional representations of the curved panels in which the panels have been flattened out. The dots in these figures represent negative radial displacements. These figures clearly show the troughs in the bifurcated panel.

Eigenvectors

The eigenvectors shown in Figs. 7 thru 12 do not display the expected results of a panel loaded in pure shear. The expected results would have the displacement troughs running diagonally across the entire element like those shown in Fig 6. The computed eigenvectors show this trend for a portion of the panel but not for the entire height. This is attributed to the shell analysis of the curved panels resulting in different internal stress distributions than those for a flat plate.

This different stress distribution is shown in Fig. 13. These zones of resultant stress distributions were found to be consistant in all the panel configurations examined. Figure 14 shows the principal stress conversions from the various computed stress states showen in Fig. 13. These principal stresses explain most of the eigenvectors showen in Figs. 7 thru 12. This is done keeping in mind the troughs will run perpendicular to the compressive load line of action. Two zones, however, are not explained by this.

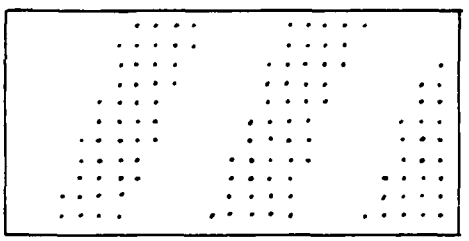

Aspect Ratio-0.5

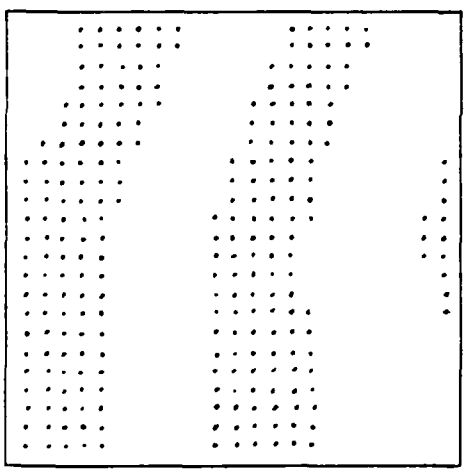

Aspect Ratio-1.0

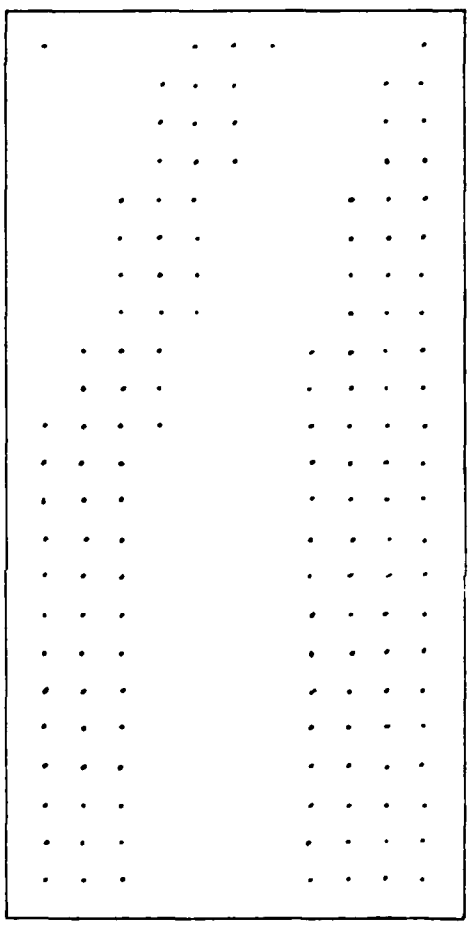

Aspect Ratio-2.0

Figure 7. Eigenvectors for Graphite/Epoxy $[0,\pm45,90]_s$. Dots Represent Negative Radial Displacements.

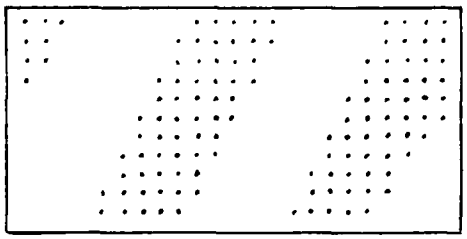

Aspect Ratio-0.5

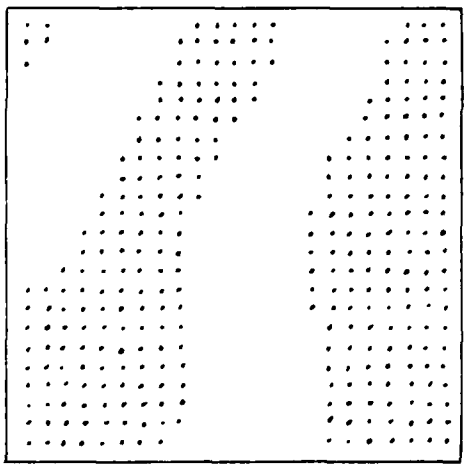

Aspect Ratio-1.0

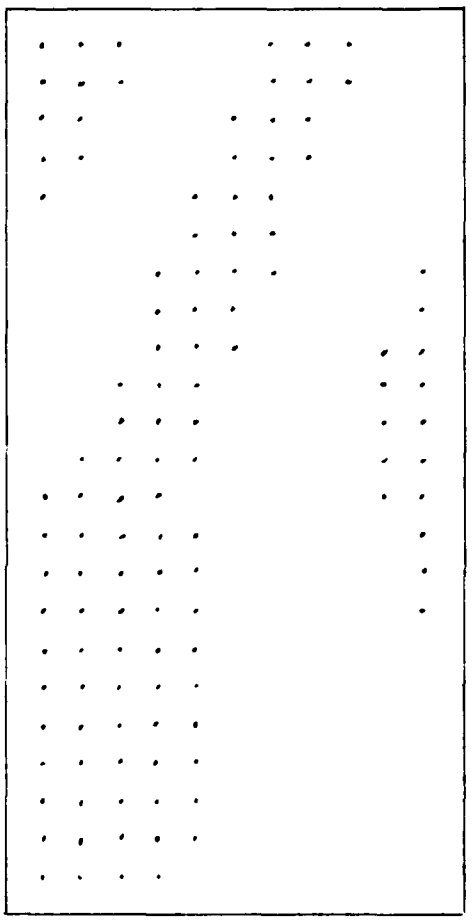

Aspect Ratio-2.0

Figure 8. Eigenvectors for Graphite/Epoxy $[0,90]_{2S}$. Dots Represent Negative Radial Displacements.

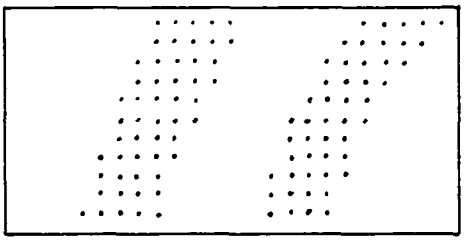

Aspect Ratio-0.5

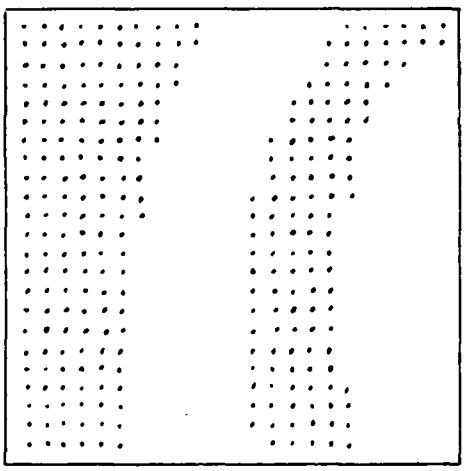

Aspect Ratio-1.0

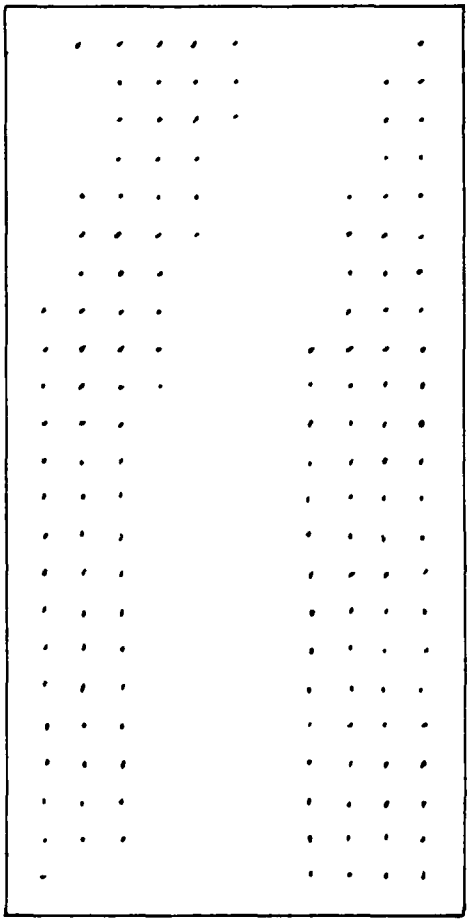

Aspect Ratio-2.0

Figure 9. Eigenvectors for Graphite/Epoxy $[\pm 45]_{2s}$. Dots Represent Negative Radial Displacements.

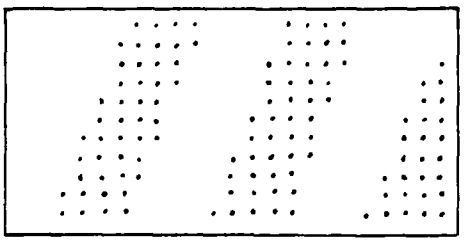

Aspect Ratio-0.5

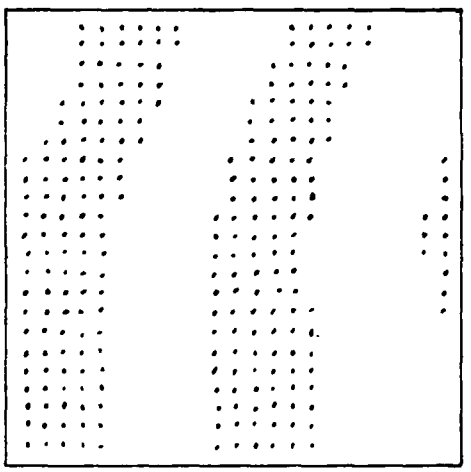

Aspect Ratio-1.0

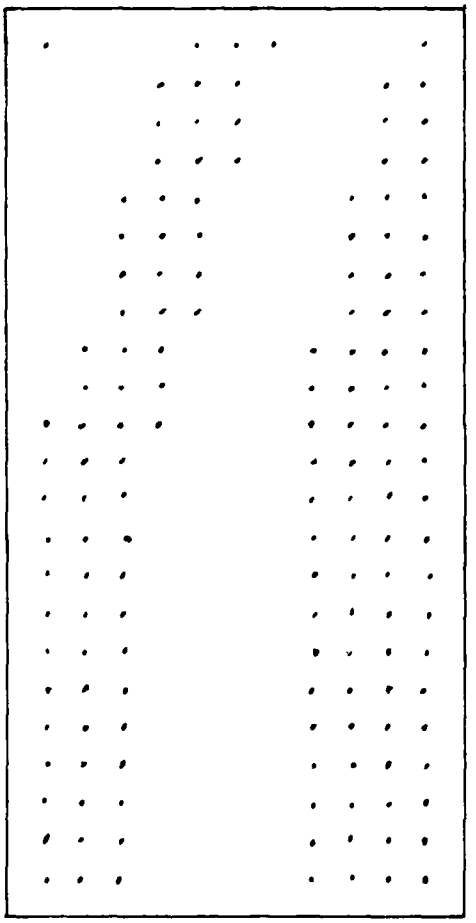

Aspect Ratio-2.0

Figure 10. Eigenvectors for Kevlar/Epoxy $[0,\pm 45,90]_s$. Dots Represent Negative Radial Displacements.

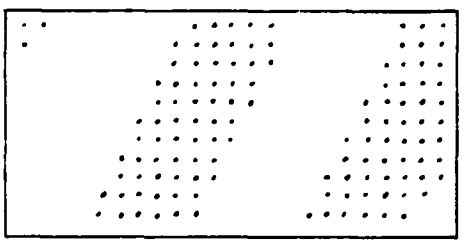

Aspect Ratio-0.5

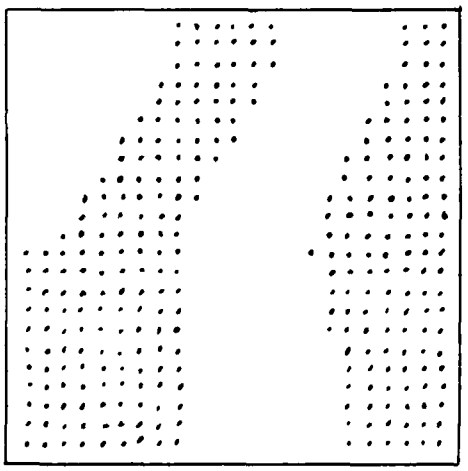

Aspect Ratio-1.0

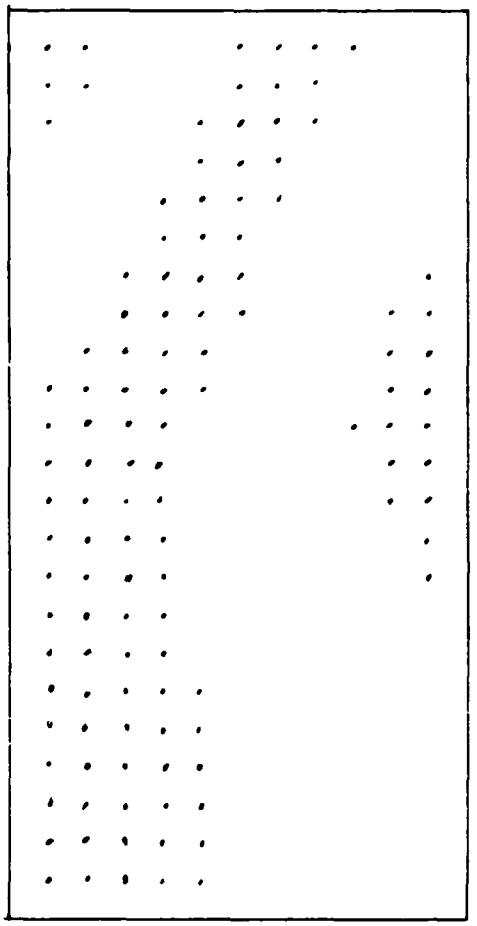

Aspect Ratio-2.0

Figure 11. Eigenvectors for Kevlar/Epoxy $[0,90]_{2s}$. Dots Represent Negative Radial Displacements.

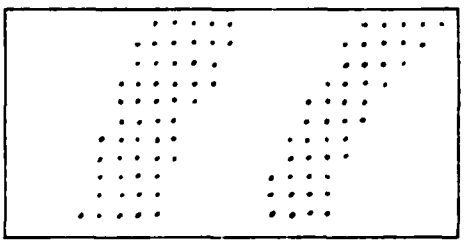

Aspect Ratio-0.5

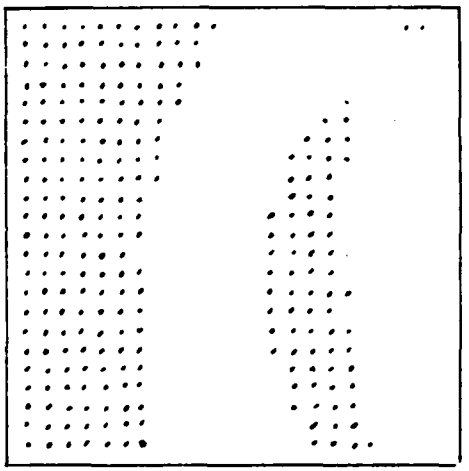

Aspect Ratio-1.0

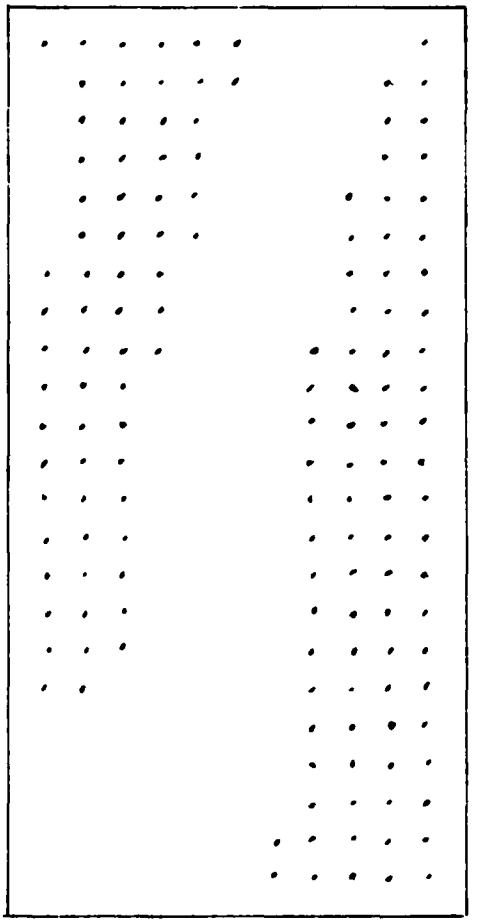

Aspect Ratio-2.0

Figure 12. Eigenvectors for Kevlar/Epoxy $[\pm 45]_{2s}$. Dots Represent Negative Radial Displacements.

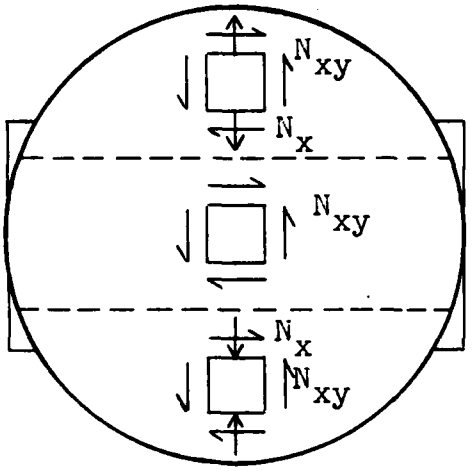

Aspect Ratio-0.5

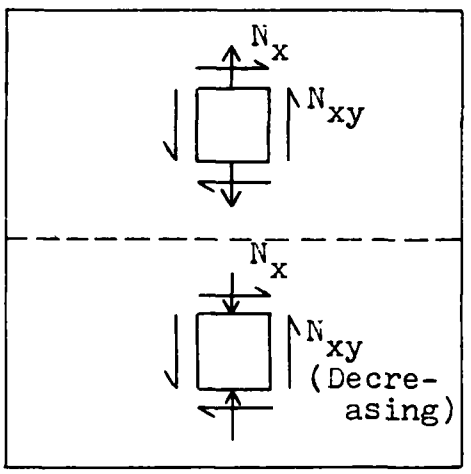

Aspect Ratio-1.0

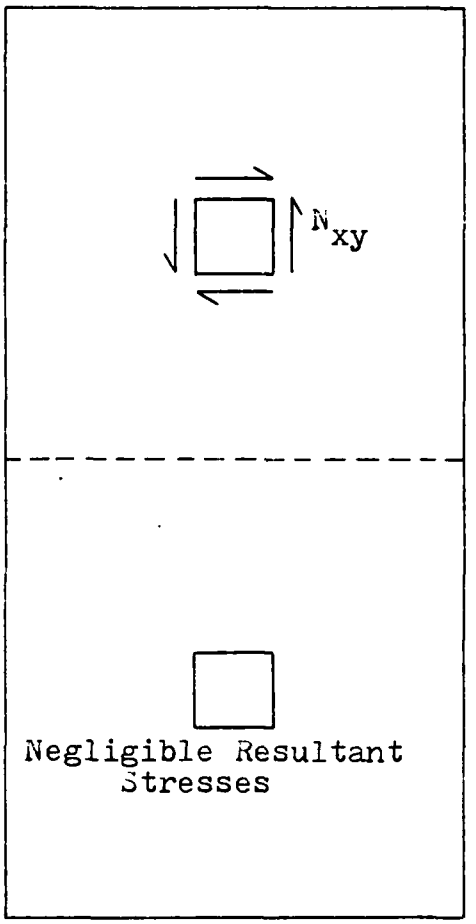

Aspect Ratio-2.0

Figure 13. N_x, N_y, and N_{xy} Distribution Throughout Panels from Computer Analysis

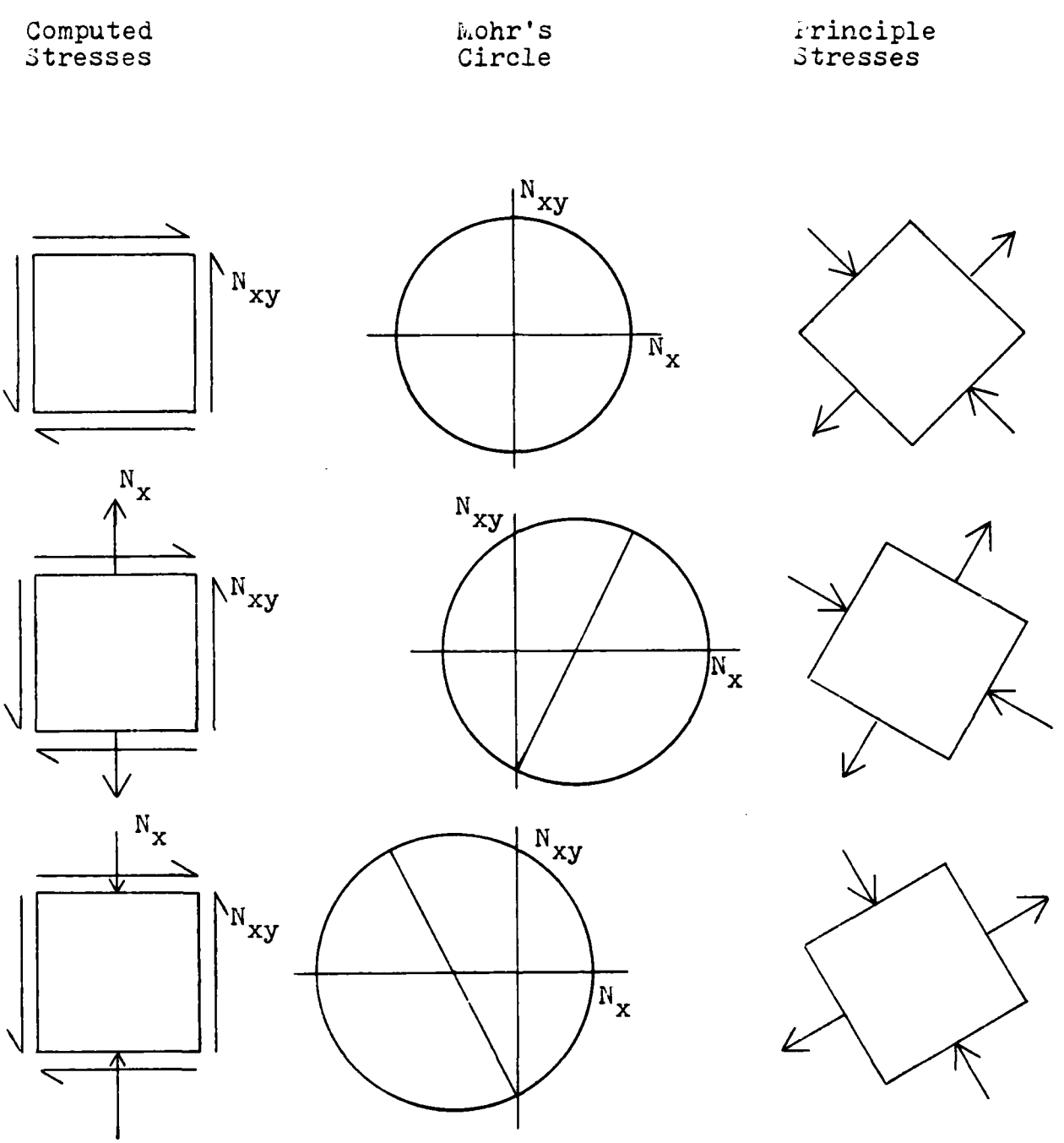

Figure 14. Transformation of Computed Stresses to Principle Stresses

These two zones, the lower half of both the panels of aspect ratio one and two, can be explained by referring to Fig. 15. This figure shows the prebifurcation radial displacements of the graphite/epoxy $[0,+45,-45,90]_S$ panel for an example. Since Fig. 13 shows no stresses in the lower portion of the panel with an aspect ratio of two, the radial displacements after bifurcation will be the same as the radial displacement before bifurcation. This is the case on comparison of Figs. 7 and 15.

Explaining the lower portion of the panels with an aspect ratio of one is not as clear. Figures 13 and 14 would indicate the eigenvector should be oriented at some angle to the horizontal other than the 90° indicated in Fig. 7. This must be due to an interaction between the prebifurcation radial displacements and those that occur after bifurcation. It was observed that the prebifurcation radial displacements were, in general, small in comparison to the shape of the bifurcation displacements. This generalized comparison is not true for the lower portion of the panels of aspect ratio one. This is attributed to the decreasing magnitude of N_{xy} in this region. Therefore, the bifurcation eigenvector will be made up of a combination of the prebuckeled and bifurcation radial displacements.

The different stress distributions for the different aspect ratios can be qualitativly explained by considering the boundary conditions used and the applied load. Since the only load that is actually applied to the panel is the line load along the top of the curved panel, a twist is applied to the panel. This twist

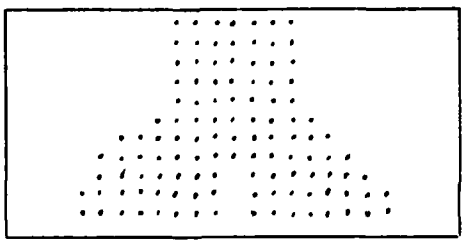

Aspect Ratio-0.5

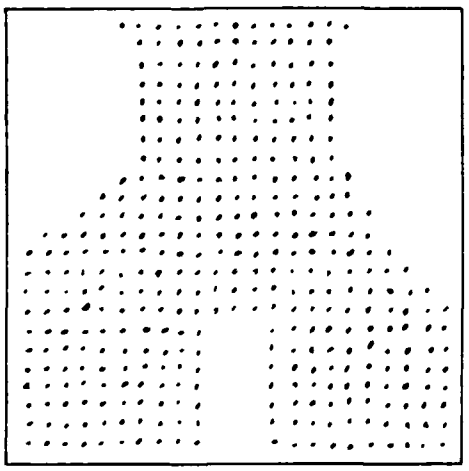

Aspect Ratio-1.0

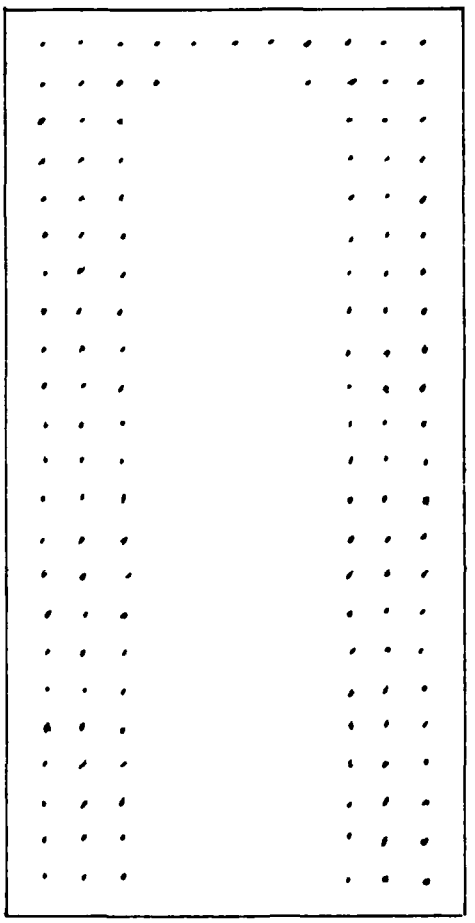

Aspect Ratio-2.0

Figure 15. Prebifurcation Radial Displacements of Graphite/Epoxy $[0,\pm 45,90]_s$ Panel. Dots Represent Negative Radial Displacements.

results in the panel trying to warp. This is something that is not seen with flat panels. This warping is the panel trying to equilibriate the N_x resultant force. Since the boundary conditions in this analysis restricted vertical displacements on the vertical edges, this warping was restricted and increasses the membrane stresses. This results in the resultant N_x force throughout the panels.

The reason the aspect ratio effects this N_x distribution is the coupling between the vertical side boundary conditions and the applied load and the fixed bottom. The panel with an aspect ratio of one has the greatest distribution of the N_x resultant force. This is due to the vertical boundaries and the top load/fixed bottom being in closest proximity. As the aspect ratio decreasses to 0.5, the top load and bottom move closer together but the vertical boundaries move proportionatly further appart. The converse is true when the aspect ratio increases to two. This indicates a smaller resultant N_x force influence on the aspect ratio 0.5 and 2.0 then with an aspect ratio of 1.0 which is the case.

The above discussion verifies that a curved panel analysed as a shell and loaded in pure shear do not react as a flat plate subjected to the same load arrangement.

Nondimensionalization Analysis

Material Analysis. The first analysis was done to remove the material property dependence on the bifurcation load. It was expected that the shear modulus of elasticity, G_{12}, would be

useful in accomplishing this. As such, the bifurcation load (remember, this load is dimensionally, force/unit length) was divided by G_{12} and the circumferential length of 12 inches. The circumferential length was used instead of the variable height because the resulting value is plotted against the aspect ratio. These results are shown in Fig. 16.

The resulting plots show clearly that this assumption relative to G_{12} is in error. The curves for the two materials do not display sufficient correlation to justify the conclusion that the shear modulus, G_{12}, is the proper material property for this analysis.

Instead of using G_{12}, the extensional modulus of elasticity, E_1 was used. Again, the bifurcation load was divided by E_1 and the circumferential length. The results of this analysis are shown in Fig. 17. This analysis provided a relationship with reasonably close correlation.

The only area where this correlation is not very close is with the $[0,90]_{2s}$ panel with aspect ratio greater than one. The load carrying capability of this panel with an aspect ratio of two is about the same as that of a panel with an aspect ratio of one. This can be explained by referring back to Fig. 13 and the stiffness coiefficints, D_{16} and D_{26}, given in Appendix B. Since D_{16} and D_{26} have values of zero for this lamina orientation, these panels can only resist shear along a 45° diagonal. However, these panels have great stiffness in the axial directions. Thus, the bifurcation of these panels will be due to the shear load and not the axial components of load. Keeping this in mind, Fig. 13

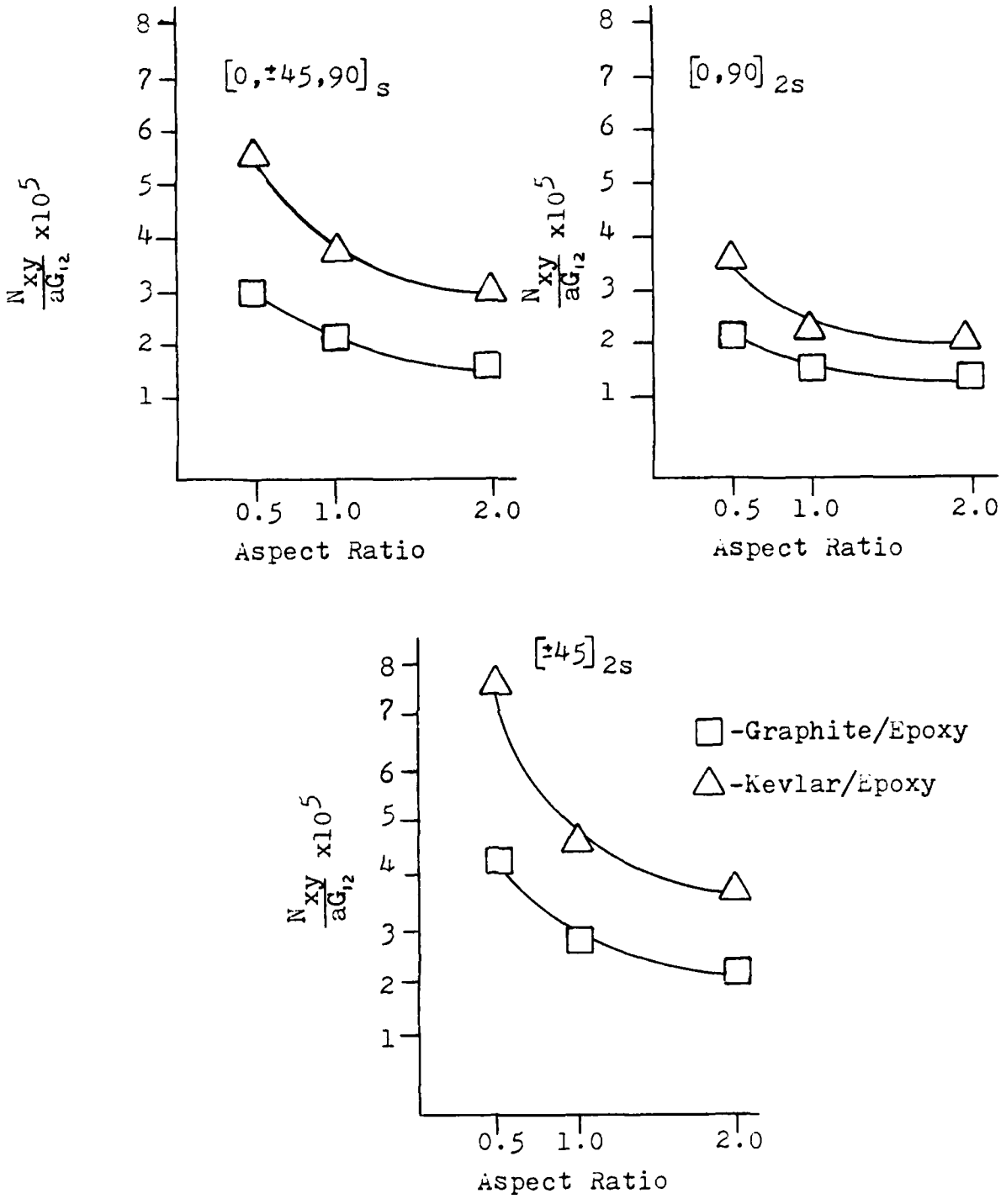

Figure 16. Effect of G_{12} on Bifurcation Load

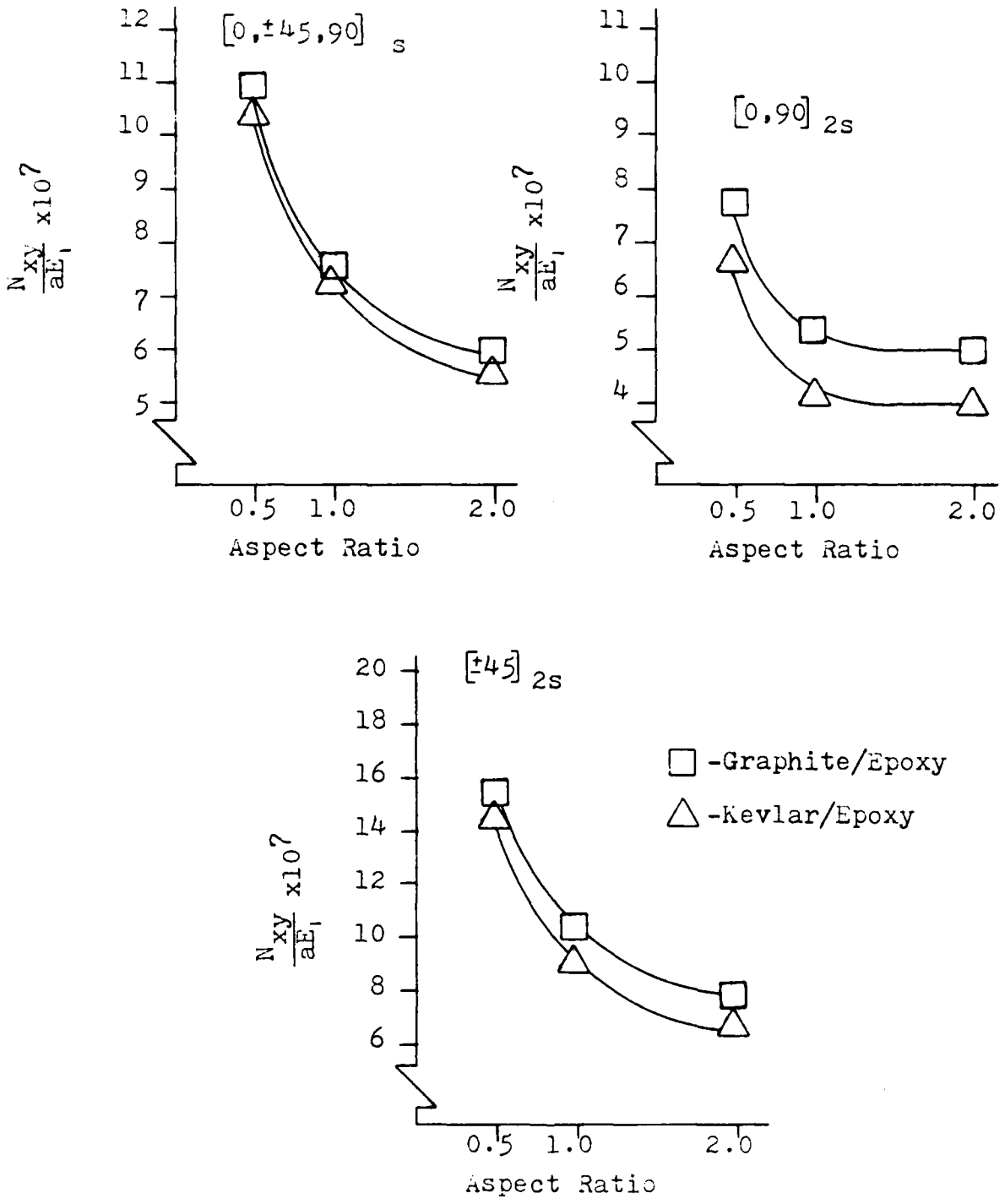

Figure 17. Effect of E_1 on Bifurcation Load

shows a very similar relationship of stress distribution over the same total area between the panels with an aspect ratio of one and two. Hence, the bifurcation load should be similar.

It is also apparent in Fig. 17 that the curves are not linear. This is again due to the fact that as aspect ratio decreases, the line load carrying capability will go to infinity since edge length is approaching zero. Conversllly, as the aspect ratio increases, edge length goes to infinity and thus the line load carrying capabiliy goes to zero. Furthermore, the various membrane resultant forces are affecting the linear relations of load versus aspect ratios.

This technique of using the Young's modulus to remove material property dependence from buckling analysis is also used in Ref. [13]. In this reference the transverse modulus, E_2 , was used as opposed to the longitudnal modulus, E_1 , as used here. Examining the moduli of the two materials used in this thesis reveals that E_1(Gr-Ep)/E_1(Ke-Ep) and E_2(Gr-Ep)/E_2(Gr-Ep) are the same. Hence, Fig. 17 would have the same trend, just different magnitude.

Qualitativly, there is a reason for the extensional modulus being the important maerial property for shear buckling analysis for these panels when shear buckling is considered in isotropic materials. As shown in Fig. 14, the failure mode for shear loading is actually a compresive failure i an off axis direction. For an isotropic material this compresion faiure is resisted by E. Since the $[0,+45,-45,90]_s$ panel is quasi-isotropic, it will also have this trait. Looking back at Fig. 17 showes that this

panel results in the best correlation. The other two panels stiffness properties move further away from quasi-isotropic and thus have a lower degree of correation.

Aspect Ratio Analysis. This analysis was accomplished by normalizing the bifurcation loads to the bifurcation loads of the panels with an aspect ratio of one. In Fig. 18 these normalized loads are plotted against aspect ratios. The result is a relationship having all the lamina orientations in close agreement with each other, even between materials. The only point out of agreement is the $[0,90]_{2s}$ panel above an aspect ratio of one. This can again be attributed to, as in the discussion on material properties, the fact that the failure mode is the same over the same total area for panels of both an aspect ratio of one and two. This again results in a bifurcation load for these two aspect ratios to be very similar.

Also, the curves in Fig. 18 are nonlinear for the same reason as given in the discussion on material properties and will not be repeated here.

An explanation of the close correlation shown in Fig. 18 is that the percentage change in bifurcation load in any ply lay-up is constant no matter what ply layup is being considered. This is obviously not the case with the $[0,90]_{2s}$ orientation for the reasons outlined above. A more complete understanding will require more lay-ups to be analysed.

Lamina Orientation Analysis. The last parameter to be studied is the effect of lamina orientation on bifurcation load. This analysis again normalized all the bifurcation loads to a

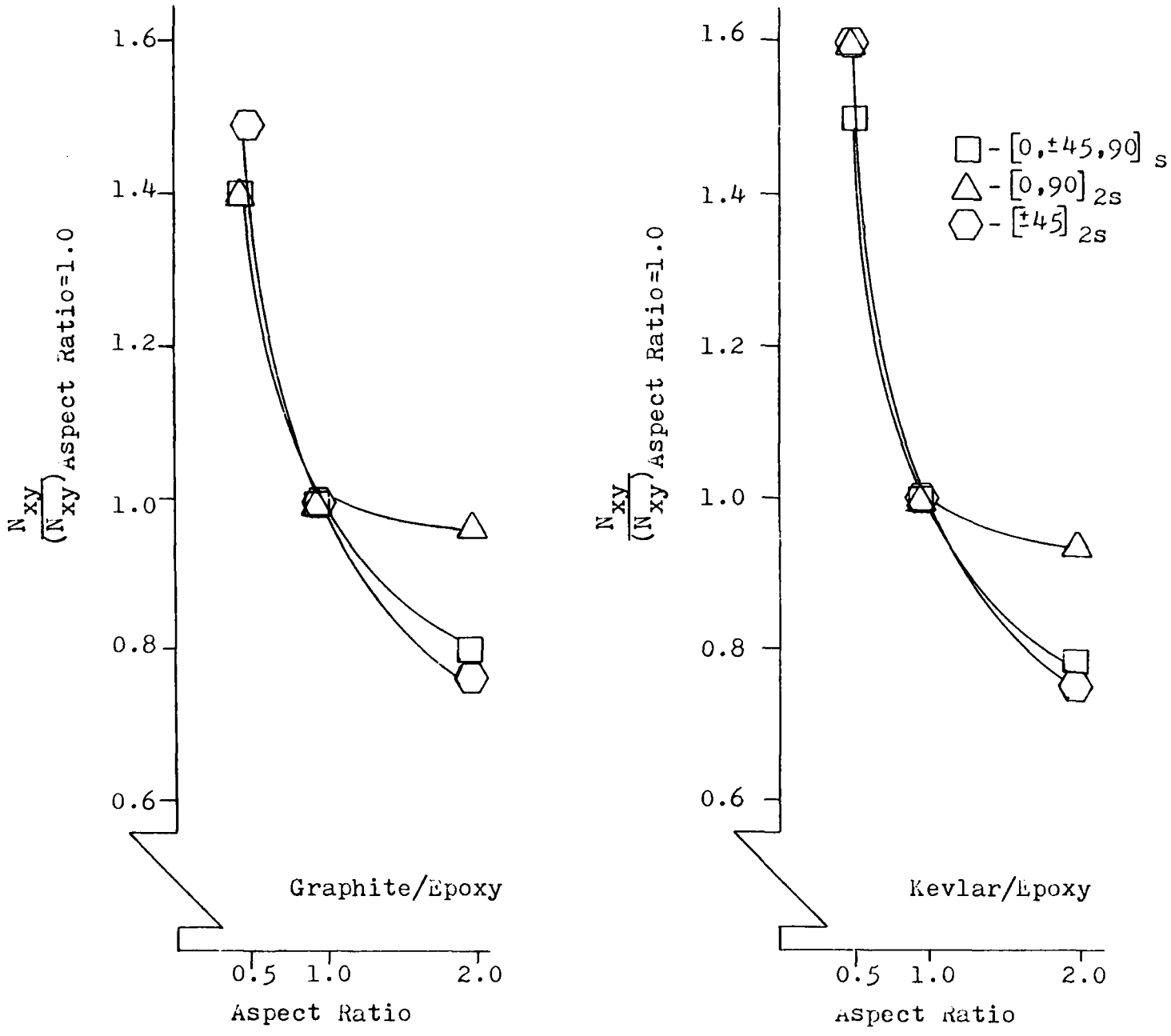

Figure 18. Effect of Aspect Ratio on Bifurcation Load

standard load. This time the bifurcation loads were normalized to the bifurcation loads of the $[0,90]_{2s}$ panels. The parameter these normalized loads were plotted against were the coupling bending stiffness terms D_{16} and D_{26}.

These stiffness terms were used because they are the ones that mostly resist shear buckling loads [10]. The values for these stiffness terms can be found in Appendix B for all the lamina orientations.

The results of this analysis are shown in Fig. 19. The trends are linear with the dependence on aspect ratios 0.5 and 1.0 removed. The panels with an aspect ratio of two do not follow this trend. This is due again to the fact that these panels do not carry all their load in pure shear. Since this is the case, the bending stiffness terms, D_{16} and D_{26} are not the values these bifurcation loads should be plotted against. Instead, a combination of bending stiffnesses D_{16}, D_{26}, and D_{66} as well as axial extension A_{16}, A_{26}, and A_{66} should be used.

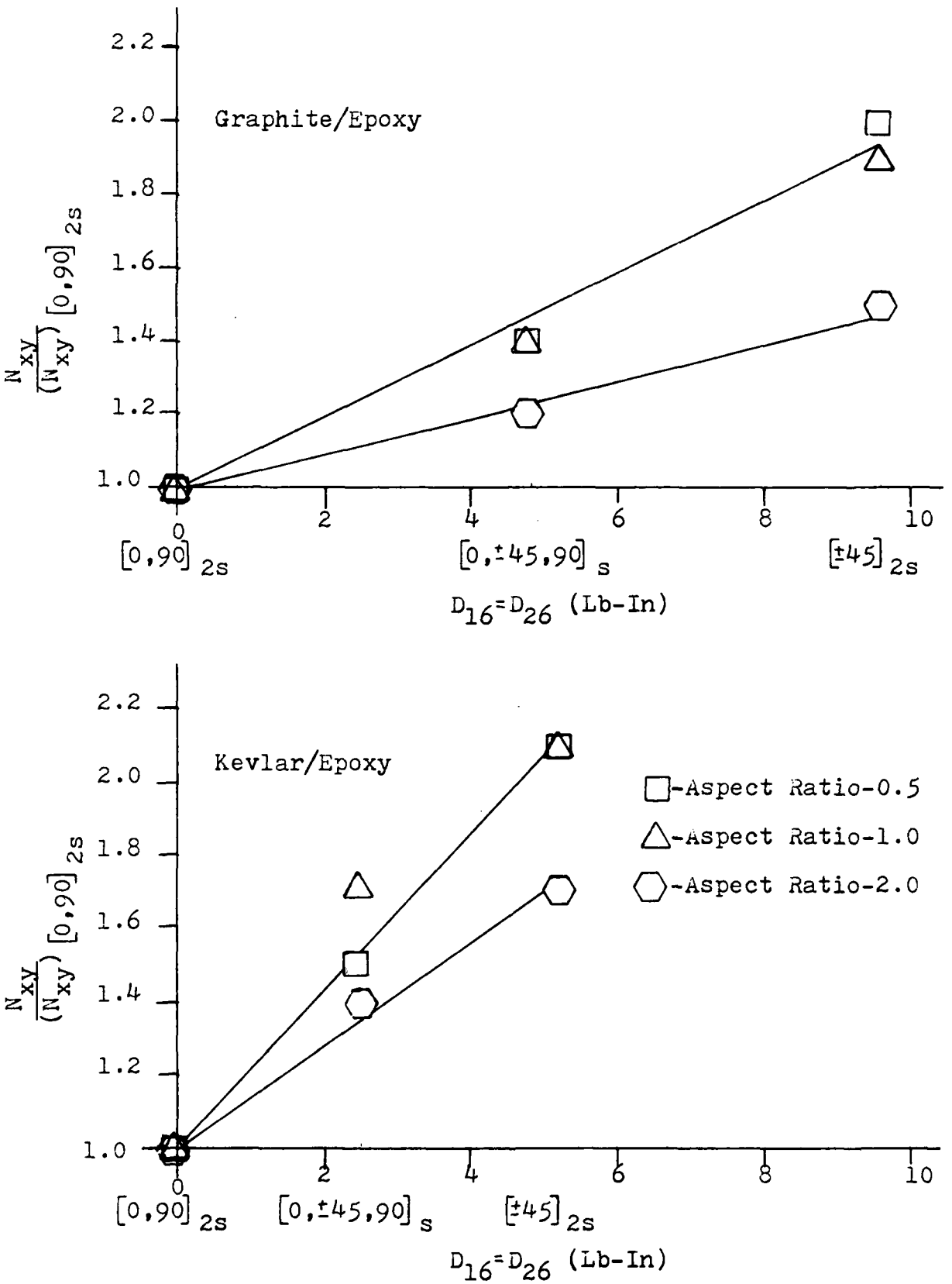

Figure 19. Effect of Lamina Orientation on Bifurcation Load

V. Conclusions

Based on the analysis completed in this thesis the following conclusions have been made:

1. The boundary conditions used in this thesis are valid for applying a pure shear load to a flat plate for a STAGSC-1 computer analysis.

2. Curved panels that are analysed as shells loaded under pure shear develop an interior shear distribution unlike that of flat plates under the same load configuration.

3. The Young's modulus, E_1 or E_2 , is a better indicator of shear stiffness than the shear modulus, G_{12} for the composite panels analysed.

4. As aspect ratios approach zero, the bifurcation load approaches infinity. Conversllly, as the aspect ratio approaces infinity, the bifurcation load generally approaches zero.

5. A panel with a ply orientation of $[0,90]_{2s}$ has approximately a constant load carrying capability above an aspect ratio of one.

6. A panel's aspect ratio effects the interior distribution of stresses.

7. The bending stiffness coefficients, D_{16} and D_{26} , effect the load carrying capability of a curved composite panel as they do for flat plates. This effect results in a higher load carrying capability for higher values of D_{16} and D_{26} .

Bibliography

1. Harper, 2Lt James G., Buckling Analysis of Laminate Composite Circular Cylindrical Shells, MS Thesis, AFIT/GAE/AA/78D-8, School of Engineering, Air Force Institute of Technology (AU), Wright-Patterson AFB OH, December 1978.

2. Hebert, Capt John S., Analytical/Experimental Linear Bifurcation of Curved Cylindrical Composite Panels, MS Thesis, AFIT/GAE/AA/82D-14, School of Engineering, Air Force Institute of Technology (AU), Wright-Patterson AFB OH, December 1982.

3. Janisse, Capt Thomas C., A Parametric Study of Surface Imperfections and Small Cutouts in a Composite Panel, MS Thesis, AFIT/GAE/AA/82D-15, School of Engineering, Air Force Institute of Technology (AU), Wright-Patterson AFB OH, December 1982.

4. Lee, Capt Catherine E., Numerical Determination of the Effects of Boundary Conditions on the Instability of Composite Panels with Cutouts, MS Thesis, AFIT/GA/AA/83D-4, School of Engineering, Air Force Institute of Technology (AU), Wright-Patterson AFB OH, December 1983.

5. Almroth, B. O., and Brogan, F. A., The STAGS Computer Code, NASA Contractor Report 2950, NASA, February 1978.

6. Almroth, B. O., Structural Analysis of General Shells Volume II User Instructions for STAGSC-1, LMSC-D633873, Applied Mechanics Laboratory, Lockheed Palo Alto Research Laboratory, Palo Alto Ca, January 1983.

7. Sobel, L. H. and Thomas, Kevin, Evaluation of the STAGSC-1 Shell Analysis Computer Program, WARD-10881. Westinghouse Advanced Reactors Division, Madison PA, August 1981.

8. Almroth, B. O. and Brogan, F. A., "Bifurcation Buckling as an Approximation of the Collapse Load for General Shells," AIAA Journal, 10: 463-467 (April 1972).

9. Bauld, N. R., Jr. and Satyamurthy, K., Collapse Load Analysis for Plates and Shells, AFFDL-TR-79-3038. Air Force Flight Dynamics Laboratory, Wright-Patterson AFB OH, December 1970.

10. Jones, Robert M., Mechanics of Composite Materials, New York: McGraw-Hill Book Company, 1975.

11. Cook, Robert D., Concepts and Applications of Finite Element Analysis (Second Edition), New York: John Wiley and Sons, 1981.

12. Ashton, J. E. and Whitney, J. M., Theory of Laminated Plates (Progress in Materials Science Series, Volume IV), Stamford: Technomic Publishing Company, 1970.

13. Whitney, James M., "Buckling of Anisotropic Laminated Cylindrical Plates," AIAA Journal, 22, 1641-1645 (November 1984).

14. Foral, R. F. and Humphrey, W. D., "Combined Stress Behavior of Graphite and Kevlar 49 Fiber/Epoxy Composites and Hybrids," AIAA Structres, Structural Dynamics, & Materials Conference, Part 1, 1982.

Appendix A

Sample Input

An example of an input deck used in this thesis is shown in Fig. 1-A. A detailled discription of each input line is given in Ref. 6. Special caution must be taken when inputing Poission's ratio. Most material property tables give ν_{12}, but the STAGSC-1 code uses ν_{21}.

```
LINEAR SHEAR ANALYSIS, ASPECT RATIO 1.0, GR-EP, 0,+45,-45,90[S]
1 $ B-1 LINEAR STATIC ANALYSIS
1 0 $ B-2 1 SHELL 0 ELEMENTS
1 0 1 0 $ B-3 1 MATERIAL 1 SHELL WALL
1.0 $ C-1 LOAD MULTIPLIER RECORD
1 0 650 $ D-2 EIGENVALUE CONTROL CARD
5 $ D-3 CLUSTER DEFINITION RECORD
25 25 $ F-1 25 ROWS 25 COLUMNS
1 0 $ I-1 MATERIAL NUMBER
20.5E06 0.0212429 .75E06 0.0 1.0 1.3E06 1.0 $ I-2 MATERIAL
     PROPERTIES
1 1 8 $ K-1 WALL CONFIGURATION
1 .005 0.0 $ K-2 PLY MATERIAL, THICKNESS, ORIENTATION
1 .005 45.0 $ K-2
1 .005 -45.0 $ K-2
1 .005 90.0 $ K-2
1 .005 90.0 $ K-2
1 .005 -45.0 $ K-2
1 .005 45.0 $ K-2
1 .005 0.0 $ K-2 END OF ALL 8 PLYS
5 $ M-1 CYLINDRICAL SHELL UNIT
0.0 12.0 0.0 57.296 12.0 $ M-2A SHELL GEOMETRY
1 0 $ M-5 SHELL WALL RECORD
411 $ N-1 ELEMENT NUMBER
0 0 0 0 $ P-1 BOUNDRY CONDITIONS SPECIFIED ON P-2 RECORD
010 011 $ P-: V, RV, RW FREE ON TOP
010 101 $ P-2 V, RU, RW FREE RT SIDE
000 011 $ P-2 RV, BW FREE ON BOTTOM
010 101 $ P-2 V, RU ,RW FREE LT SIDE
1 $ Q-1 1 LOAD SYSTEM
1 4 0 $ Q-2 1 LOAD SET SYSTEM A
1.0 2 2 1 $ Q-3 TOP LINE LOAD
-1.0 3 0 0 13 $ Q-3 RIGHT LINE LOAD
-1.0 2 2 13 $ Q-3 BOTTOM LINE LOAD
1.0 3 1 0 1 $ Q-3 LEFT LINE LOAD
1 1 0 0 $ R-1 PRINT OUTPUT
```

Figure 1-A. Sample STAGSC-1 Input

Appendix B

Stiffness Coeficients

The following are the extensianal and bending stiffness coeifficient matrices for the panels investigated in this thesis. The equations given in chapter two were used with the material properties given in chapter three. Note that since the panels are all symmetric, the coupling stiffness matrix is the null matrix.

Graphite-Epoxy

$[0,+45,-45,90]_S$

$$A=\begin{bmatrix}0.35 & 0.11 & 0.00\\ 0.11 & 0.35 & 0.00\\ 0.00 & 0.00 & 0.12\end{bmatrix} \times 10^6 \text{ \#/in} \qquad D=\begin{bmatrix}77.0 & 12.0 & 4.80\\ 12.0 & 20.0 & 4.80\\ 4.80 & 4.80 & 14.0\end{bmatrix} \text{ \#-in}$$

$[0,90]_{2S}$

$$A=\begin{bmatrix}0.44 & 0.02 & 0.00\\ 0.02 & 0.44 & 0.00\\ 0.00 & 0.00 & 0.03\end{bmatrix} \times 10^6 \text{ \#/in} \qquad D=\begin{bmatrix}77.0 & 2.30 & 0.00\\ 2.30 & 39.0 & 0.00\\ 0.00 & 0.00 & 4.00\end{bmatrix} \text{ \#-in}$$

$[+45,-45]_{2S}$

$$A=\begin{bmatrix}0.26 & 0.20 & 0.00\\ 0.20 & 0.26 & 0.00\\ 0.00 & 0.00 & 0.21\end{bmatrix} \times 10^6 \text{ \#/in} \qquad D=\begin{bmatrix}34.0 & 26.0 & 9.60\\ 26.0 & 34.0 & 9.60\\ 9.60 & 9.60 & 28.0\end{bmatrix} \text{ \#-in}$$

Kevlar-Epoxy

$[0,+45,-45,90]_s$

$$A = \begin{bmatrix} 0.18 & 0.06 & 0.00 \\ 0.06 & 0.18 & 0.00 \\ 0.00 & 0.00 & 0.06 \end{bmatrix} \times 10^6 \ \#/in \qquad D = \begin{bmatrix} 40.0 & 6.30 & 2.50 \\ 6.30 & 9.50 & 2.50 \\ 2.50 & 2.50 & 6.60 \end{bmatrix} \ \#\text{-in}$$

$[0,90]_{2s}$

$$A = \begin{bmatrix} 0.23 & 0.01 & 0.00 \\ 0.01 & 0.23 & 0.00 \\ 0.00 & 0.00 & 0.01 \end{bmatrix} \times 10^6 \ \#/in \qquad D = \begin{bmatrix} 40.0 & 0.80 & 0.00 \\ 0.80 & 20.0 & 0.00 \\ 0.00 & 0.00 & 1.10 \end{bmatrix} \ \#\text{-in}$$

$[+45,-45]_{2s}$

$$A = \begin{bmatrix} 0.12 & 0.11 & 0.00 \\ 0.11 & 0.12 & 0.00 \\ 0.00 & 0.00 & 0.11 \end{bmatrix} \times 10^6 \ \#/in \qquad D = \begin{bmatrix} 17.0 & 14.0 & 5.10 \\ 14.0 & 17.0 & 5.10 \\ 5.10 & 5.10 & 15.0 \end{bmatrix} \ \#\text{-in}$$

VITA

Captain Jay K. McDaniel was born on 29 April 1957 in Flint, Michigan. He graduated from high school in Grand Blanc, Michigan, in 1975 and attended Michigan Technological University from which he received the degree of Bachelor of Science in Mechanical Engineering in May 1979. Upon graduation, he received a commission in the USAF through the ROTC program. He was then assigned to the Air Force Rocket Propulsion Laboratory, Liquid Rocket Division at Edwards AFB, California as a rocket propulsion engineer. He then entered the School of Engineering, Air Force Institute of Technology, in May 1983.

Permanent adress: 12003 S. Saginaw St.
Bldg. 6, Apt. 1
Grand Blanc, Michigan 48439

UNCLASSIFIED
SECURITY CLASSIFICATION OF THIS PAGE

REPORT DOCUMENTATION PAGE

1a. REPORT SECURITY CLASSIFICATION: UNCLASSIFIED	1b. RESTRICTIVE MARKINGS
2a. SECURITY CLASSIFICATION AUTHORITY	3. DISTRIBUTION/AVAILABILITY OF REPORT: Approved for public release; distribution unlimited.
2b. DECLASSIFICATION/DOWNGRADING SCHEDULE	
4. PERFORMING ORGANIZATION REPORT NUMBER(S): AFIT/GA/AA/84D-5	5. MONITORING ORGANIZATION REPORT NUMBER(S)
6a. NAME OF PERFORMING ORGANIZATION: School of Engineering; 6b. OFFICE SYMBOL (If applicable): AFIT/EN	7a. NAME OF MONITORING ORGANIZATION
6c. ADDRESS (City, State and ZIP Code): Air Force Institute of Technology, Wright-Patterson AFB, Ohio 45433	7b. ADDRESS (City, State and ZIP Code)
8a. NAME OF FUNDING/SPONSORING ORGANIZATION; 8b. OFFICE SYMBOL (If applicable)	9. PROCUREMENT INSTRUMENT IDENTIFICATION NUMBER
8c. ADDRESS (City, State and ZIP Code)	10. SOURCE OF FUNDING NOS. — PROGRAM ELEMENT NO. / PROJECT NO. / TASK NO. / WORK UNIT NO.
11. TITLE (Include Security Classification): See Box 19	
12. PERSONAL AUTHOR(S): Jay K. McDaniel, Capt, USAF	
13a. TYPE OF REPORT: MS Thesis; 13b. TIME COVERED: FROM _____ TO _____; 14. DATE OF REPORT (Yr., Mo., Day): 1984 December; 15. PAGE COUNT: 66	
16. SUPPLEMENTARY NOTATION	

17. COSATI CODES		
FIELD	GROUP	SUB. GR.
11	04	

18. SUBJECT TERMS (Continue on reverse if necessary and identify by block number): Composite Materials, Shear Buckling, Finite Elements, Bifurcation Analysis, Curved Panels

19. ABSTRACT (Continue on reverse if necessary and identify by block number)

Title: ANALYTICAL SHEAR BUCKLING INVESTIGATION OF CURVED COMPOSITE PANELS

Thesis Chairman: Dr. Anthony Palazotto

(See Back)

20. DISTRIBUTION/AVAILABILITY OF ABSTRACT: UNCLASSIFIED/UNLIMITED ☒ SAME AS RPT. ☐ DTIC USERS ☐	21. ABSTRACT SECURITY CLASSIFICATION: UNCLASSIFIED
22a. NAME OF RESPONSIBLE INDIVIDUAL: Dr. Anthony Palazotto	22b. TELEPHONE NUMBER (Include Area Code): 513-255-3517; 22c. OFFICE SYMBOL: AFIT/ENY

DD FORM 1473, 83 APR EDITION OF 1 JAN 73 IS OBSOLETE.

UNCLASSIFIED
SECURITY CLASSIFICATION OF THIS PAGE

Abstract:

This numerical investigation paremetrically determined how material and geometric properties affect the buckling load capability of 8-ply curved composite panels loaded under pure shear. The linear bifurcation capabilities of the STAGSC-1 finite element computer code developed by the Lockheed Palo Alto Research Laboratory was employed. Results from this computer code were compared with other published analytical results of similar configuration to verify boundary conditions.

Representitive material properties for both graphite-epoxy and Kevlar-epoxy were used. The aspect ratios of 0.5, 1.0, and 2.0 were achieved by varying the axial length of the cylindrical panel. Both quasi-isotropic and symmetric orthotropic fiber orientations were analysed.

Results indicate that these curved composite panels, while loaded with a shear load resulting in pure shear reactions in flat plates, do not react in pure shear. Once the interior force resultants are established, the load carrying capability of the curved panels follow classical laminated plate theory.

END

FILMED

5-85

DTIC